

1  
2  
3 **Mechanical, durability, depolluting and electrical properties of**  
4 **multifunctional mortars prepared with commercial or waste carbon-based**  
5 **fillers**  
6  
7

8 Alessandra Mobili<sup>1</sup>, Alberto Belli<sup>2</sup>, Chiara Giosuè<sup>1</sup>, Mattia Pierpaoli<sup>3</sup>, Luca Bastianelli<sup>4</sup>, Alida  
9 Mazzoli<sup>1</sup>, Maria Letizia Ruello<sup>1</sup>, Tiziano Bellezze<sup>1</sup>, Francesca Tittarelli<sup>1,5</sup>

10 <sup>1</sup>*Department of Materials, Environmental Sciences and Urban Planning (SIMAU), Università*  
11 *Politecnica delle Marche, via Brecce Bianche 12, 60131, Ancona, Italy –INSTM Research Unit.*

12 <sup>2</sup>*Department of Applied Science and Technology (DISAT), Politecnico di Torino, INSTM Research*  
13 *Unit, Corso Duca degli Abruzzi 24, 10129, Torino, Italy*

14 <sup>3</sup>*Department of Metrology and Optoelectronics, Faculty of Electronics, Telecommunication and*  
15 *Informatics, Gdansk University of Technology, 80-233 Gdansk, Poland*

16 <sup>4</sup>*Department of Information Engineering (DII), Università Politecnica delle Marche, via Brecce*  
17 *Bianche 12, 60131, Ancona, Italy.*

18 <sup>5</sup>*ISAC – CNR, via Piero Gobetti 101, 40129, Bologna, Italy.*

19  
20 Corresponding author: Tel.: +39 071 2204726.

21 E-mail address: [a.mobili@univpm.it](mailto:a.mobili@univpm.it) (A. Mobili).  
22

23 **Highlights**

- 24 • Commercial and waste carbon-based fillers are compared in lime-based mixes  
25 • Waste fillers increase the compressive strength of lime-based mixes  
26 • Waste fillers decrease lime-based mixes water suction and increase VOCs adsorption  
27 • Waste fillers increase electrical conductivity and EMI SE of lime-based mixes  
28 • Waste fillers are a sustainable and cheap alternative for multifunctional mixes

## 30 **Abstract**

31 Carbon-based fillers from industrial wastes and commercial ones were compared to improve the  
32 properties of lime-based mixes. As commercial fillers, graphene nanoplatelets and activated carbon  
33 were used, whereas as industrial wastes a char obtained by the gasification of biomasses and a used  
34 foundry sand were chosen. Carbon-based wastes were found to be a good cost-effective alternative  
35 to commercial carbon based fillers to increase the compressive strength (of about 25%) and to reduce  
36 water capillary absorption (of about 50%) thanks to the paste refinement; to enhance depollution  
37 capacity (of about 25%) and increase both electrical conductivity (up to 65%) and electromagnetic  
38 shielding effectiveness (of about 6%) of the hardened compounds thanks to the carbon content.

39

## 40 **Keywords**

41 Mortar, Multifunctionality, Carbon-based filler, Mechanical properties, Durability, Depollution,  
42 Electrical properties.

43

## 44 **1. Introduction**

45 In the last two decades, carbon-based commercial fillers as carbon black, graphene and its derivatives  
46 (carbon nanotubes, fullerenes, etc.), and carbon nanofibers have been studied as possible additions in  
47 binder-based matrices in order to improve their multifunctionality. As a matter of fact, thanks to their  
48 high mechanical strength, high specific surface area, porosity, lightness, and high electrical  
49 conductivity [1,2] they can enhance the mechanical, durability, depolluting and especially electrical  
50 and electromagnetic properties of mortars and concretes [3–7].

1 In particular, air pollution, related to the dispersion in atmosphere of particulate matters (PMs),  
2 nitrogen oxides (NO<sub>x</sub>), and volatile organic compounds (VOCs), is a serious problem not only for  
3 outdoor but also for indoor environments where respiratory diseases and the so-called “Sick Building  
4 Syndrome” can affect the health of occupants [8] since people spend about 90% of their time in



55 confined environments [9]. Also electromagnetic (EM) radiations generated by electronic devices  
56 and communication systems, particularly at high frequencies, can be dangerous for humans [10,11],  
57 besides interfering with other electronic devices [12–14].

58 A possible solution to these issues can be the development of multifunctional building materials that  
59 can both decrease the concentration of air pollutants and reduce the spreading of EM signals in  
60 confined environments. Indeed, considering air depollution, up to now, several indoor air cleaning  
61 technologies have been improved; not only active technologies, which are energy consuming, as  
62 filtration, non-thermal plasma and electrostatic precipitator [15] but also more sustainable passive  
63 technologies, that can interact with the active technologies minimizing the energy consumption, using  
64 construction materials as substrates for adsorption and photocatalysis have been developed. In  
65 particular, adsorption can occur on highly porous materials, with high specific surface area (300-3000  
66 m<sup>2</sup>/g) [16], and photocatalysis can mineralize pollutants into less harmful compounds by means of a  
67 nano-catalyst, such as titanium dioxide (TiO<sub>2</sub>) activated under UV-A radiation [17]. Construction  
68 materials can also reduce passively the spreading of EM signals if, again, a high specific surface area  
69 with porous materials is guaranteed since it enhances the electromagnetic shielding property [18] of  
70 materials, that is the property to reflect and/or absorb electromagnetic radiations.

71 So far, carbonaceous fillers addition has been extensively studied in binder-based materials.

72 Activated carbon is one of the most efficient adsorptive materials for gases and vapours (VOCs or  
73 NO<sub>x</sub>) in air or pollutants in water both if used as it is [19,20] or if it is dispersed within a matrix  
74 [21,22]. The effectiveness depends on its wide surface area, porosity and chemical functional group  
75 that can act even in a binding matrix. Researchers have been also studied low-cost alternatives such  
76 as from waste precursor [23]. Activated carbon, can also enhance the electromagnetic shielding  
7 effectiveness of construction materials through the multiple reflections phenomenon [24].

8 Graphene and its derivatives, because of their high specific surface area, are suitable for gas sorption  
9 materials [25]. Le et al. [2] proved that GNP is able to enhance the electrical conductivity of cement-  
0 based composites and if GNP content exceeds the percolation value (the limit beyond which the



81 conductive particles touch each other), the moisture content does not influence the electrical  
82 conductivity. Liu et al. [26] reported that GNP is better than graphene oxide nanoplatelets (GONP)  
83 to manufacture electrically conductive cement-based materials. Moreover, GNP is reported to be  
84 suitable also to produce mortars with piezoresistive behaviour [27,28], thus the material changes its  
85 electrical resistivity if subjected to strain [29,30].

86 However, the essential prerequisite for the efficient use of carbon-based fillers to enhance multi-  
87 functionality of binder-based composites is their good dispersion in the mix. Unfortunately, carbon-  
88 based commercial fillers can be barely dispersible in polar liquids like water, since, due to their high  
89 specific surface area, Van der Waals' forces create bundles and agglomerates. Moreover, many  
90 commercial carbon-based materials as graphene nanoplatelets (GNP) and carbon nanotubes are  
91 highly expensive and some of them, as carbon black or carbon nanotubes, are very toxic [31,32].

92 Cost can be saved by using carbon-based industrial by-products obtained by the thermal treatment of  
93 biomasses that are much cheaper, being wastes, than commercial ones. Moreover, thanks to a  
94 different chemical composition with the presence of functional groups formed by other elements than  
95 carbon (as Mg, Al, Ca, Si, Na, K, Fe, O), they result more compatible with water and then easily  
96 dispersible in polar liquids [33].

97 Char is an industrial by-product obtained by treating biomasses at high temperatures, as in the  
98 gasification process. Gasification takes place at  $T = 500-1400\text{ }^{\circ}\text{C}$  and the resulting char is a highly  
99 porous material mainly composed by carbon [34]. A recent paper by Sirico et al. [35] reports that the  
100 addition of char from gasification to mortars at 1 wt.% by cement maintains both the compressive  
101 and flexural strengths similar to those of control specimens by slightly increasing the fracture energy.

102 Some studies have confirmed that thermal treated biomasses or waste biomass ashes can enhance the  
3 absorption of VOCs [36,37] and can be a potential low-cost substitutes of activated carbon for air  
4 depollution [34]. Moreover, the high carbon content makes char a good candidate also for enhancing  
5 the electromagnetic shielding effectiveness and electrical properties of construction materials.



106 Used foundry sand is another industrial by-product obtained by the ferrous and non-ferrous metal  
107 casting industries where it is used as a moulding casting material because of its great thermal  
108 conductivity. The addition of used foundry sand has been already studied in cement-based  
109 mortars/concretes; however, its use has been mainly focused as substitute of natural sand [38,39].  
110 Used foundry sand has a high silica content, but contains also carbonaceous additions and several  
111 metals [40]. Also in this case, the carbonaceous additions and the elevated metal content make this  
112 by-product a good candidate to enhance the electromagnetic shielding effectiveness and electrical  
113 properties of construction materials.

114 Therefore, in this paper, two commercial carbon-based fillers, graphene nanoplatelets and powdered  
115 activated carbon, and two different low cost waste carbonaceous fillers, a char from gasification of  
116 biomasses and the finest fraction of a used foundry sand, have been compared as addition to enhance  
117 the mechanical, durability, depolluting, and electrical properties of pastes/mortars. As binder, a  
118 hydraulic lime was chosen, since lime-based mortars are extensively used as renders/panels in indoor  
119 applications. Moreover, hydraulic lime mortars are commonly used for rehabilitation of historical  
120 buildings due to their compatibility with the substrate, where instead cement-based mortars are not  
121 allowed, and lime is a more sustainable binder than ordinary Portland cement [41]. Literature reports  
122 only few articles on the effect of carbon-based fillers on the properties of lime-based mortars:  
123 graphene oxide added at 0.05 and 0.1 wt.% by lime [42] and the replacement of lime with waste  
124 graphite powder up to 25 wt.% [43] are able to increase the mechanical performance of mortars by  
125 decreasing their porosity. A recent paper published by some of the present authors has focused on the  
126 use of gasification char and used foundry sand at 1.0% on the total volume as alternatives to graphene  
127 nanoplatelets to decrease the electrical resistivity of cement-based mortars [44]. In the paper, it was  
8 found that gasification char is better than used foundry sand to enhance some properties of cement  
9 mortars since it decreases by 42% their electrical resistivity and by 17% their capillary water  
0 absorption. However, to the best of authors' knowledge, there are no paper dealing with the use of  
1 gasification char and used foundry sand as carbonaceous by-products for enhancing properties of



132 hydraulic lime-based mixes. Moreover, in the present paper lime-based pastes have been subjected to  
133 investigation, to enhance the effect of additions on the matrix since, as reported in [45], aggregates  
134 can act as an obstacle in the electric current path increasing the electrical resistivity of concrete.

135

## 136 2. Experimental

### 137 2.1 Materials

138 Natural hydraulic lime (NHL 5, according to UNI EN 459-1) was used as binder.

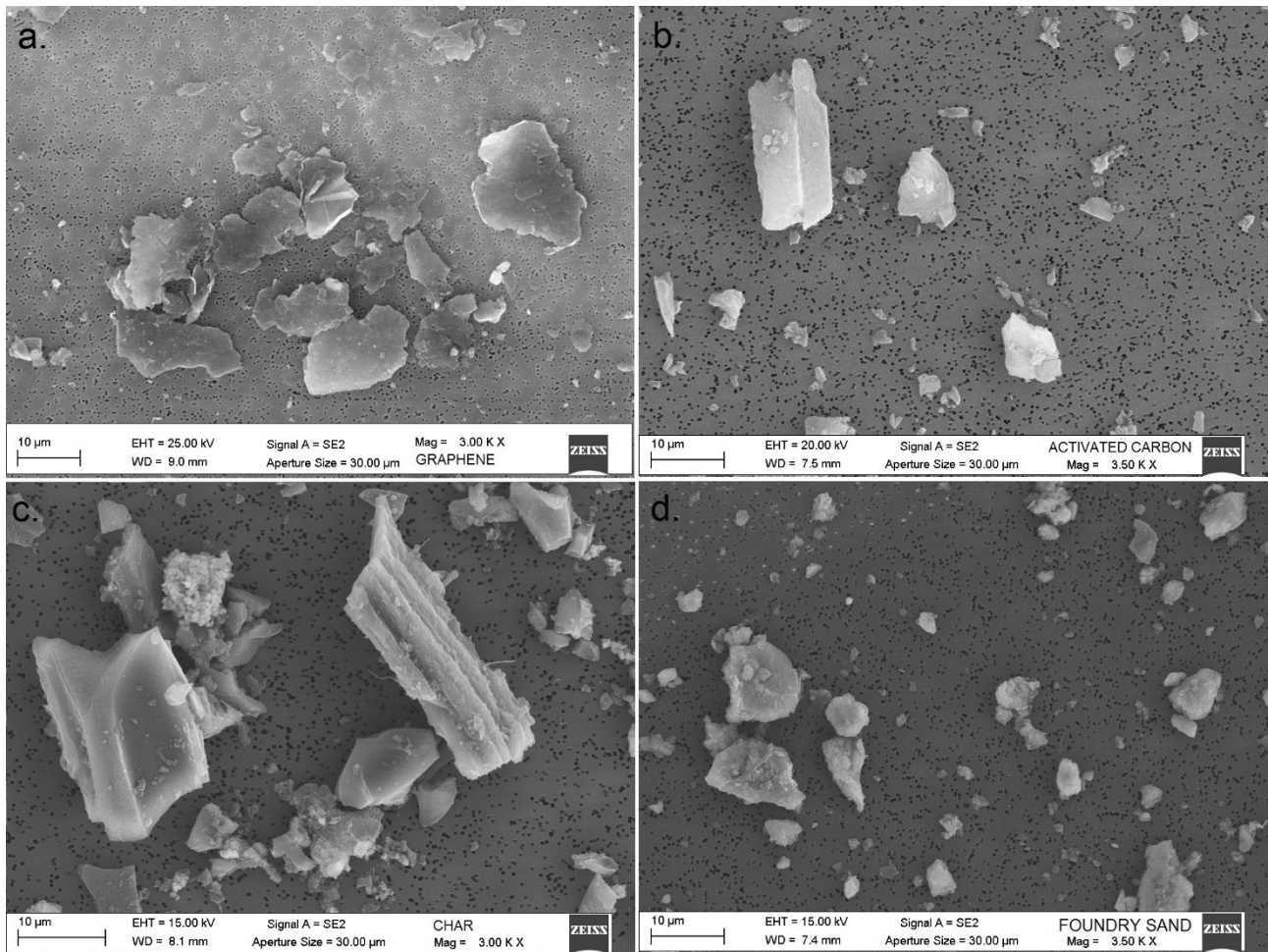
139 As commercial carbon-based fillers, graphene nanoplatelets (GNP) (Pentagraf, Pentachem S.r.l.),  
140 with a thickness of 6 – 8 nm and a width lower than 5  $\mu\text{m}$  and activated carbon (AC) (Norit® CAP  
141 SUPER-WJ, Cabot Norit Nederland B.V.) with a mean particle size of 20  $\mu\text{m}$  were used. GNP has a  
142 BET surface area of 30  $\text{m}^2/\text{g}$ , whereas AC has a BET surface area of 1800  $\text{m}^2/\text{g}$ .

143 As waste fillers, a char (CH) from biomasses gasification, provided by a plant located in central Italy,  
144 and the finest fraction of a used foundry sand (FS), provided by the Italian company LA.BO S.r.l.  
145 were used. In particular, CH is obtained by the gasification (Holz-Kraft, Spanner Re<sup>2</sup> GmbH gasifier)  
146 of natural wood chips, after to be dried to a moisture content lower than 13%. CH and FS were ground  
147 and sieved in order to have a particle size distribution lower than 75  $\mu\text{m}$ . CH and FS have a BET  
148 surface area of 76  $\text{m}^2/\text{g}$  and 341  $\text{m}^2/\text{g}$ , respectively. The full characteristics of CH and FS are reported  
149 in [44].

150 The morphology of the fillers analysed by Scanning Electron Microscopy (SEM) and the  
151 corresponding elemental analysis obtained by EDX-Analysis are given in Fig. 1 and Table 1,  
152 respectively. The SEM images highlight the flat shape of GNP (Fig. 1a), the spherical shape of FS  
153 (Fig. 1d) and the more elongated aspect of both AC and CH fillers (Figs. 1b and 1c, respectively).







155

156

157

158

159

160

161

**Fig. 1.** SEM of carbonaceous fillers: a. graphene nanoplatelets (GNP); b. activated carbon (AC); c. char (CH) from gasification minor of 75 µm; d. foundry sand (FS) minor of 75 µm.

**Table 1.** Elemental analysis of waste carbonaceous fillers (wt.%).

Filler	C	O	Ca	K	Mg	Si	Al	Na	Fe
GNP	99.50	0.50	-	-	-	-	-	-	-
AC	95.23	4.77	-	-	-	-	-	-	-
CH	76.72	14.93	5.39	2.04	0.57	0.36	-	-	-
FS	32.92	37.87	1.91	0.66	1.18	14.83	6.38	1.97	2.28

SEM and ImageJ processing software have been used to evaluate the morphology of the particles and to measure both the particle size and size distribution of AC and CH. An image analysis method was conducted, since indirect advanced methods (e.g. those involving scattered, diffracted light or laser) assume the particle being spherical, which was not the predominant case of AC and CH (Figs. 1b and 1c). In fact, for those particles that show an irregular shape, assuming them to be regular and

166 geometrical will result in an oversimplification. The irregular particles have been described by the  
167 diameter of a circle of equal projection area ( $d_{EC}$ ), Feret's diameter ( $d_F$ ) and minimal Feret's diameter  
168 ( $Min d_F$ ), on the basis of previous researches carried out by the authors [46,47].

169

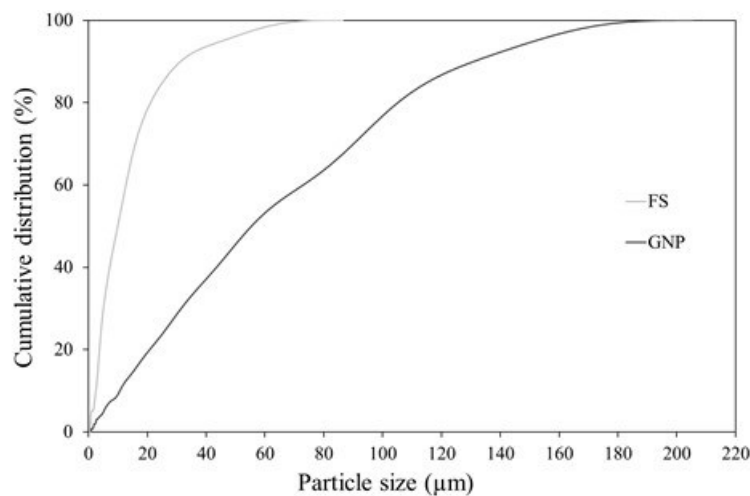
170 **Table 2.** Mean values and standard deviations of  $d_{EC}$ ,  $d_F$  and  $Min d_F$  for CH and AC samples.

Sample	$d_{EC}$ ( $\mu\text{m}$ )	$d_F$ ( $\mu\text{m}$ )	$Min d_F$ ( $\mu\text{m}$ )
CH	$1.6 \pm 2.5$	$2.5 \pm 3.5$	$1.5 \pm 2.3$
AC	$2.8 \pm 3.2$	$4.7 \pm 4.5$	$2.9 \pm 3.0$

171

172 In the case of GNP and FS, the particle size distribution was determined by laser diffraction analysis,  
173 since both showed a predominant spherical morphology (Figs. 1a and 1d). Results are showed in Fig.  
174 2: FS sieved at 75  $\mu\text{m}$  is finer than GNP, which shows also a broader grain size distribution.

175



176

177 **Fig. 2.** Particle size distribution of graphene nanoplatelets (GNP) and foundry sand (FS) with particle  
178 size distribution lower than 75  $\mu\text{m}$ .

179

## 0 *2.2 Preparation of the dispersion*

1 To better disperse each carbonaceous addition, fillers were put into different solutions, composed by  
2 water or by water and superplasticiser. Three different samples were prepared: one containing water  
3 and GNP and two containing water, superplasticiser and GNP. Two types of liquid superplasticiser





184 were compared: a naphthalene sulphonate superplasticiser (N200) (Mapefluid N200, Mapei S.p.A.)  
185 and an acrylic superplasticiser (SP1) (Dynamon SP1, Mapei S.p.A.). N200 and SP1 were added in  
186 two different amounts, namely 0.5 wt.% and 1.0 wt.% of the binder, whereas GNP was added at 0.5  
187 wt.% of the binder. Initially, the compounds were manually stirred for 1 minute; then, they underwent  
188 to sonication with an ultrasonicator for 10 minutes at 20 °C (the complete characteristics of the  
189 ultrasonicator are reported below). The quality and stability of the dispersions were evaluated by  
190 means of a portable turbidimeter (Orbeco-Hellige Model 966) after set periods of time, namely  
191 immediately after sonication and after 5, 15, 30, 60 and 120 minutes. Also the amount and type of  
192 superplasticiser for preparing the final mixtures were chosen after the evaluation of GNP dispersion  
193 by means of the turbidimeter. The turbidimeter works with a light beam which passes through the  
194 sample, if there are suspended particles the light is scattered. The dispersions were evaluated in terms  
195 of turbidity, which describes the cloudiness of a fluid caused by large numbers of individual particles,  
196 generally invisible to the naked eye. The turbidity is measured by Nephelometric Turbidity Units  
197 (NTU); if a substance is completely dissolved in solution, light is nearly no scattered leading to a low  
198 NTU value, whereas if the solubility limit is reached and the substance starts to precipitate, the light  
199 is strongly scattered leading to a high NTU value.

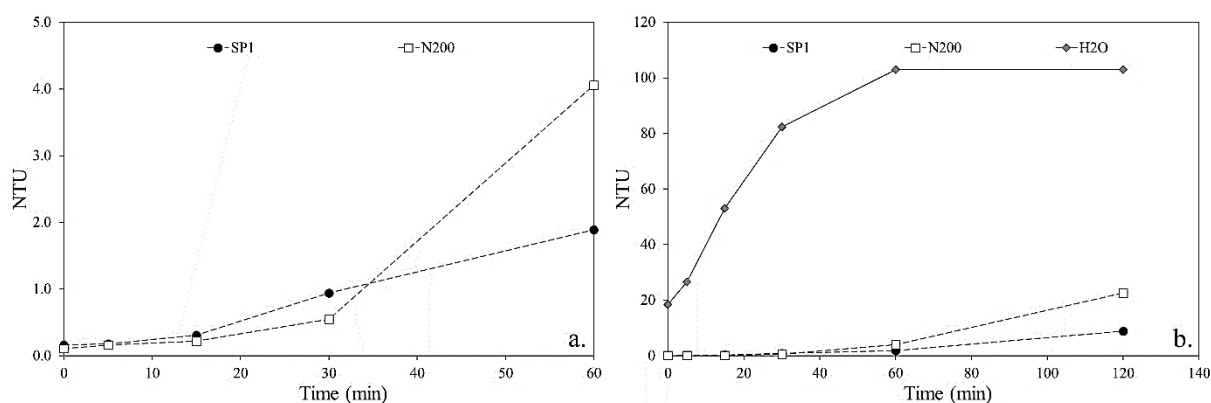
200 When SP1 and N200 were added to 0.5 wt.% of the binder, the NTU values after sonication were  
201 1.30 and 1.00, whereas after 5 minutes 2.00 and 1.40, respectively. On the other hand, when SP1 and  
202 N200 were added to 1.0 wt.% of the binder, after sonication the NTU values were 0.16 and 0.11,  
203 whereas after 5 minutes 0.18 and 0.16, respectively. The slightly lower NTU values obtained by  
204 samples prepared with N200 compared to those containing SP1 mean that N200 is better than SP1 to  
205 disperse GNP. Moreover, when the superplasticiser is added at 1.0 wt.%, the dispersion is more  
6 homogeneous than when added at 0.5 wt.%; for this reason, it was decided to use the superplasticiser  
7 at 1.0 wt.% on the binder.

8 The turbidity levels of the dispersions prepared with the sole water and with 1.0 wt.% of  
9 superplasticisers in time are reported in Fig. 3. Immediately after sonication, the dispersion of GNP



210 prepared with N200 obtained a lower NTU value compared to that prepared with SP1. This condition  
211 is maintained for the first 30 minutes after sonication, whereas later the two curves invert (Fig. 3a)  
212 and SP1 becomes the one which ensures the best dispersion up to 2 hours of sonication (Fig. 3b). On  
213 the other hand, when water alone is used as dispersant (H2O curve), the dispersion has a much higher  
214 NTU value, which is maintained for all the duration of the test (Fig. 3b), meaning that water alone is  
215 not effective neither to disperse GNP nor to maintain the dispersion stable after sonication.  
216 After a short period of time (30 minutes), the addition of N200 to water ensured a better dispersion  
217 of GNP compared to SP1. This is in agreement with other studies which suggest the use of  
218 naphthalene sulphonate superplasticiser as dispersing agent for carbonaceous fillers [2,48,49].

219



220

221 **Fig. 3.** Turbidity of the dispersion evaluated in terms of Nephelometric Turbidity Units (NTU) after  
222 a. 60 mins after sonication (enlargement) and b. 120 mins after sonication.

223

### 224 2.3 Preparation of specimens

225 The pastes were manufactured in order to reach a stiff consistency (flow value  $\leq 140$  mm, UNI EN  
226 1015:3), by using N200 and different amounts of carbonaceous fillers (0.25, 0.50 and 1.00 wt.% on  
7 lime). As reference (REF), a paste without filler addition was prepared. Mix proportions and  
8 workability of pastes are reported in Table 3.

9

230 **Table 3.** Mix proportions and flow values of pastes submitted to mechanical, microstructural,  
 231 capillary water absorption, electrical conductivity and depolluting tests (flow and in batch tests).

Mixtures	NHL 5 (g/L)	Water (g/L)	N200 (g/L)	GNP (g/L)	AC (g/L)	CH (g/L)	FS (g/L)	w/b	Flow value (mm)
REF	1375	441	13.75	-	-	-	-	0.32	117
GNP 0.25	1375	441	13.75	3.44	-	-	-	0.32	112
GNP 0.50	1375	441	13.75	6.87	-	-	-	0.32	112
GNP 1.00	1375	441	13.75	13.75	-	-	-	0.32	107
AC 0.25	1375	441	13.75	-	3.44	-	-	0.32	112
AC 0.50	1375	441	13.75	-	6.87	-	-	0.32	107
AC 1.00	1375	456	13.75	-	13.75	-	-	0.33	107
CH 0.25	1375	441	13.75	-	-	3.44	-	0.32	109
CH 0.50	1375	441	13.75	-	-	6.87	-	0.32	113
CH 1.00	1375	441	13.75	-	-	13.75	-	0.32	110
FS 0.25	1375	441	13.75	-	-	-	3.44	0.32	112
FS 0.50	1375	441	13.75	-	-	-	6.87	0.32	115
FS 1.00	1375	441	13.75	-	-	-	13.75	0.32	112

232

233 In order to analyse the effect of carbonaceous fillers on the depolluting activity in terms of NO<sub>x</sub>  
 234 abatement, pastes were also prepared by adding 1 wt.% on lime of a titanium dioxide photocatalytic  
 235 agent (TiO<sub>2</sub>), AEROXIDE® TiO<sub>2</sub> P 25 (Evonik Resource Efficiency GmbH). In fact, its  
 236 photocatalytic activity under UV radiation is a well-known issue [6]. Pastes compositions with TiO<sub>2</sub>  
 237 addition are reported in Table 4.

238

239 **Table 4.** Mix proportions of pastes with TiO<sub>2</sub> submitted to depolluting tests (flow test).

Mixtures	NHL 5 (g/L)	Water (g/L)	N200 (g/L)	GNP (g/L)	AC (g/L)	CH (g/L)	FS (g/L)	TiO <sub>2</sub> (g/L)	w/b
REF T	1434	545	14.34	-	-	-	-	14.34	0.39
GNP 0.50 T	1434	545	14.34	7.17	-	-	-	14.34	0.39
AC 0.50 T	1434	545	14.34	-	7.17	-	-	14.34	0.39
CH 0.50 T	1434	545	14.34	-	-	7.17	-	14.34	0.39
FS 0.50 T	1434	545	14.34	-	-	-	7.17	14.34	0.39

0

1 The electromagnetic shielding effectiveness was evaluated on mortars prepared with a water/binder  
 2 (w/b) ratio of 0.49 and a calcareous sand with a maximum grain size of 3 mm (sand/lime ratio = 3  
 3 wt.%). In order to prevent detachment or cracking of mortars due to shrinkage from the sample holder

244 used in SE measurements, a shrinkage reducing admixture (SRA) (Mapecure SRA, Mapei S.p.A.)  
 245 and a CaO expansive agent (Expancrete, Mapei S.p.A.) in amounts equal to 2 and 5 wt.% on lime,  
 246 respectively, were added to mortars. Carbon-based fillers were added at the same dosage weight of  
 247 dry materials used for pastes, namely 0.50 wt.% on lime for GNP and AC and 1.00 wt.% on lime for  
 248 CH and FS, respectively. The fillers dispersion was carried out with the same procedure used for  
 249 pastes. Mortars compositions are reported in Table 5.

250

251 **Table 5.** Mix proportions of mortars submitted to electromagnetic shielding property tests.

Mixtures	NHL 5 (g/L)	Water (g/L)	N200 (g/L)	GNP (g/L)	AC (g/L)	CH (g/L)	FS (g/L)	SAND (g/L)	CaO (g/L)	SRA (g/L)	w/b
M REF	524	256	13.75	-	-	-	-	1611	26.19	10.47	0.49
M GNP 0.50	524	256	13.75	6.87	-	-	-	1611	26.19	10.47	0.49
M AC 0.50	524	256	13.75	-	6.87	-	-	1611	26.19	10.47	0.49
M CH 1.00	524	256	13.75	-	-	13.75	-	1611	26.19	10.47	0.49
M FS 1.00	524	256	13.75	-	-	-	13.75	1611	26.19	10.47	0.49

252

253 Pastes were prepared by mixing the blend of water, N200 and filler with the lime (previously mixed  
 254 with TiO<sub>2</sub>, if necessary) until homogeneity for 3 minutes.

255 To manufacture mortars, lime was previously mixed with CaO and sand until homogeneity was  
 256 reached, and then the blend of water, superplasticiser and filler was incorporated. Finally, SRA was  
 257 added to the mortar and mixed for 3 minutes.

258 Superplasticiser was manually stirred together with the mixing water, later the carbonaceous fillers  
 259 were added to the liquid. Fillers were dispersed for 10 minutes at 20 °C by means of an ultrasonicator  
 260 Vibra Cell™ VCX 130 (Sonics & Materials, Inc.) equipped with a probe with a diameter of 13 mm  
 261 that works with a frequency of 20 kHz by setting an amplitude of 70%. Since the stability of the  
 2 dispersion with N200 is ensured during the first 30 minutes after sonication (Fig. 3a), the dispersion  
 3 was immediately mixed with dry materials for the preparation of pastes and mortars in order to avoid  
 4 a possible sedimentation of the carbon-based fillers.

265 After mixing, the workability of pastes was measured in accordance with the UNI EN 1015-3  
266 standard.

267 Pastes and mortars were poured into different moulds according to the tests to be carried out and  
268 cured at  $T = 20 \pm 1$  °C and  $RH = 95 \pm 5\%$  for 7 days and then maintained at  $T = 20 \pm 1$  °C and  $RH =$   
269  $50 \pm 5\%$  until testing.

270

## 271 *2.3 Methods*

### 272 *2.3.1 Mechanical characterization*

273 In order to investigate the effect of the fillers on the mechanical properties of the pastes (Table 3),  
274 **three specimens with 40x40x160 mm dimensions** were manufactured and submitted to both  
275 compression and tensile splitting tests after 2, 7 and 28 days of curing according to UNI EN 1015-11  
276 and UNI EN 12390-6, respectively.

277

### 278 *2.3.2 Microstructural characterization*

279 To establish the correlation of the obtained results with the microstructure, mercury intrusion  
280 porosimetry (MIP) was performed using a Thermo Fisher Pascal 240 porosimeter to analyse the pore  
281 size distribution and the total open porosity ( $V_p$ ) of pastes. **One small fragment for each composition**  
282 **(Table 3) of about 1 cm<sup>3</sup>** was tested after 28 days of curing. Moreover, SEM observations were  
283 performed using a SEM PHILIPS XL20 equipment on small samples of graphite coated paste  
284 specimens (Table 3) after 28 days of curing.

285

### 286 *2.3.3 Capillary water absorption*

7 Since water is the medium and the main carrier of aggressive ions ( $Cl^-$ ,  $SO_4^{2-}$ , etc.) [50,51], the study  
8 concerning the water absorption is of primary importance to give information on the durability of a  
9 construction material. The durability of pastes (Table 3) was studied through capillary water  
0 absorption tests by measuring the amount of water absorbed by a dried specimen through capillary



291 suction in time. For short contact periods (90 min), the capillary water absorption coefficient ( $C$ ) was  
292 calculated **on three 40x40x80 mm paste specimens per composition** according to UNI EN 1015-18  
293 **and the average result was reported**. For long contact periods, the water absorbed per unit area ( $Q_i$ )  
294 **by the same three specimens per compositions** was measured for 8 days according to UNI EN 15801.

295

#### 296 2.3.4. Depolluting Tests

297 In order to investigate if the carbonaceous fillers additions used in this research could give a certain  
298 depolluting activity to lime-based materials, the depolluting properties of different pastes were  
299 evaluated after 28 days of curing. Two different experimental tests were performed: in-batch, in order  
300 to explore the effect of different fillers on the adsorbent properties of pastes for VOCs; and in  
301 continuous, by flow test method inside a reactor, to highlight the possible effect of the carbon-based  
302 fillers on the photocatalytic ability of pastes. In flow test, pastes with and without  $\text{TiO}_2$  were  
303 characterized (Table 4 and Table 3, respectively).

304

##### 305 2.3.4.1. In batch test

306 In batch test Gas Chromatography was used for monitoring the concentration of Methyl-ethyl-ketone  
307 (MEK) against time injected in a 16.65 L sealed glass box containing the tested specimen [52]. Inside  
308 the box a fan guaranteed a continuous air recirculation. The specimens were cylinders with an exposed  
309 area of 5026  $\text{mm}^2$ . **For each composition, one specimen was tested**. Air samples inside the box were  
310 collected by a micro-syringe every 8 min and analysed with a gas chromatograph (GC 8000 Top  
311 Carlo Erba instruments®, injector split 1:15, carrier control by flow; capillary column characteristics:  
312 length 25 m, thickness 0.52  $\mu\text{m}$ ,  $\text{Ø}$  0.32 mm, crosslinked Methyl Siloxane, isotherm 50 °C, FID  
3 Detector). The initial amount of MEK injected into the test box was 50  $\mu\text{L}$  which corresponds to 2402  
4  $\text{mg}/\text{m}^3$  (approximately four times the Threshold Limit Value – TLV). The monitoring over time of  
5 data started after 20 min from the first injection to guarantee that all MEK was vaporised. Then, the  
6 results were plotted as a percentage of the concentration detected ( $C_i$ ) with respect to the initial





317 concentration ( $C_0$ ). The tests were conducted in dark condition (absence of irradiation) for 110  
318 minutes.

319

#### 320 2.3.4.2. Flow test

321 The continuous flow test was performed according to UNI 11247 [8]. The specimens, with the same  
322 dimensions of those used for the in batch test, were placed on a tripod inside a borosilicate glass  
323 chamber of 3.58 L. An UVA metal-halogen quartz lamp (power 400 W), with mercury vapour peak  
324 at 360 nm irradiated the specimen surface. The distance between the surface of the specimen and the  
325 lamp guarantees a specimen radiance of about  $20 \text{ W/m}^2$ , measured before each test [8]. The inlet gas  
326 was a mixture of synthetic air and  $\text{NO}_x$ . The chamber was linked to an analyser Monitor Labs,  
327 Nitrogen Oxides Analyser model 8841. The guaranteed inlet concentration of  $\text{NO}_x$  was 500 ppb and  
328 the abatement coefficient  $A_c$  (the percentage of  $\text{NO}_x$  abated) was evaluated according to UNI 11247.

329

#### 330 2.3.5. Electrical and electromagnetic shielding properties

331 Finally, the electrical and electromagnetic shielding properties of mortars were tested. It is well-  
332 known that electrical and electromagnetic properties are related, and generally, at the lowest electrical  
333 resistances, the best results for electromagnetic SE are found [53–55].

334

##### 335 2.3.5.1. Electrical resistivity

336 The electrical resistivity of a material can be measured by using alternating current (AC) [56] or direct  
337 current (DC) [28]. In this paper, electrical resistivity ( $\rho$ ) was determined by means of a DC four-probe  
338 approach (Fig. 4) **on three paste specimens per composition** (Table 3) at 7, 14, 21 and 28 days of  
9 curing. The four-probe approach was used to determine the potential difference across the specimens,  
0 after the application of a set constant current, and to remove the effects of electrodes polarization.  
1 During casting, two AISI 304 stainless steel sheets (30x50x1 mm) were immersed in each specimen,  
2 30 mm depth, leaving out the remaining 20 mm on the top of the surface and at a distance of 120 mm



343 each one (Fig. 4). At the same way, two AISI 304 stainless steel rods ( $\varnothing$  3 mm) were immersed in  
344 the specimens, 20 mm depth and placed at 100 mm each one, 10 mm far from the corresponding sheet  
345 at the same specimen side, as showed in Fig. 4. A constant DC current was applied by an Amel Mod.  
346 2059 potentiostat/galvanostat on the outer two stainless steel sheets, and the potential difference was  
347 measured using a high impedance digital multimeter between the inner two stainless steel rods.  
348 Since each electrolytic cell, as the lime pastes, is characterized by its own specific geometry, a cell-  
349 constant  $K$  must be determined for it, considering that this particular conductor is conforming to the  
350 second Ohm's Law:

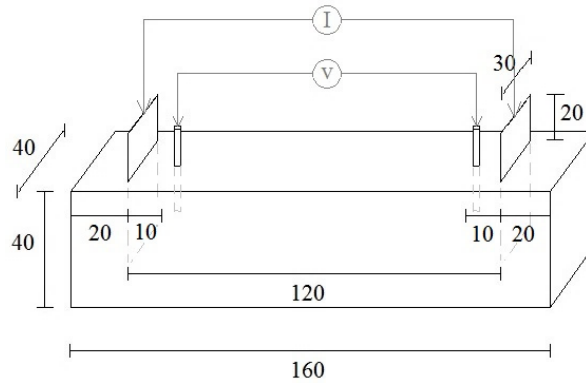
$$351 \quad R = \rho \frac{l}{A} \quad (1)$$

352 where  $R$  ( $\Omega$ ) is the resistance of the electrolytic conductor into the cell, measured between two  
353 hypothetical metallic electrodes, placed at a distance of  $l$  cm and having a contact area  $A$  ( $\text{cm}^2$ ). The  
354 cell-constant  $K$  is given by the  $l/A$  ratio ( $\text{cm}^{-1}$ ), whereas  $\rho$  ( $\Omega \cdot \text{cm}$ ) is the resistivity of the electrolytic  
355 conductor and the inverse ( $1/\rho$ ) its conductivity  $\kappa$  ( $\Omega^{-1} \cdot \text{cm}^{-1}$  or  $\text{S} \cdot \text{cm}^{-1}$ ; S = siemens). Considering that  
356 an ideal cell, with well-defined geometrical dimensions, does not exist, for real cells as showed in  
357 Fig. 4,  $K$  was determined by the immersion of the four-probes in an aqueous solution having a known  
358  $K$  value, at the same configuration showed in Figure 4. Therefore, using the same equipment  
359 described above, the resistance  $R$  was measured and  $\kappa$  was calculated using the Eq. (1). The solution  
360 used for this purpose was KCl 0.01 M, having  $\kappa = 1.408 \text{ mS} \cdot \text{cm}^{-1}$  at  $25 \text{ }^\circ\text{C}$  [57]. Actually, the  
361 conductivity of this solution was experimentally measured with an electrical conductivity meter  
362 AMEL Mod. 160 and the value  $\kappa = 1.442 \text{ mS} \cdot \text{cm}^{-1}$  was obtained.

363 In detail, in order to obtain the value of the resistance  $R$  of the cell with KCl solution for all the  
4 specimens, firstly, the potential difference ( $\Delta V_0$ ) between the two rods was measured in absence of  
5 current, then, a constant current  $I$  was applied between the two sheets in the range  $5 - 10000 \mu\text{A}$  and  
6 the new potential difference ( $\Delta V_i$ ) was measured. These measurements were plotted in a ( $\Delta V_i - \Delta V_0$ )  
7 vs  $I$  diagram (Fig. 5). Interpolating the values that showed a linear trend, the value of the electrical

368 resistance  $R$  was obtained. From this  $R$  value, a cell-constant  $K = 0.6849 \text{ cm}^{-1}$  was calculated. Using  
 369 Eq. (1) and this  $K$  value, from  $R$  determinations,  $\rho$  values were calculated for all specimens as a  
 370 function of the curing time.

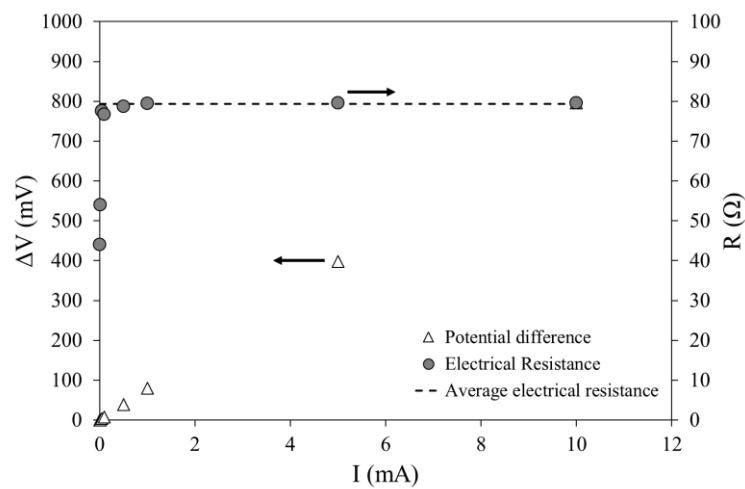
371



372

373 **Fig. 4.** Specimen scheme and electrodes configuration for DC electrical resistivity measurements.

374



375

376 **Fig. 5.** Example of the determination of the electrical resistance ( $R$ ) through potential difference ( $\Delta V_i$   
 377 -  $\Delta V_0$ ) and current ( $I$ ) measurements.

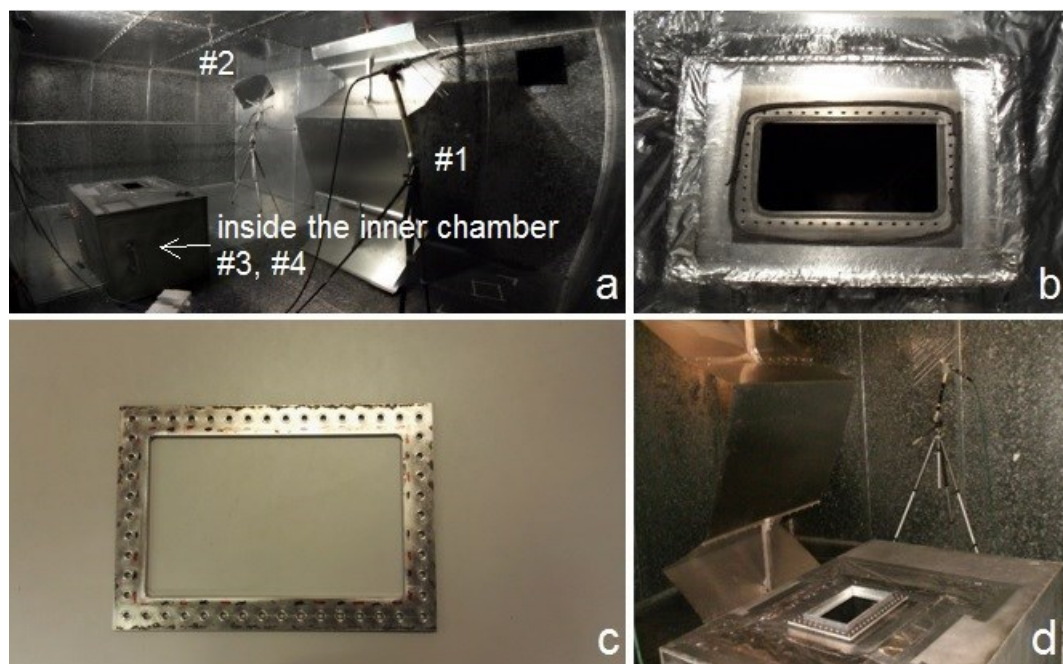
378

### 9 2.3.5.2. Electromagnetic shielding property

0 The electromagnetic shielding properties of the materials can be evaluated in diverse ways. In this  
 1 paper the use of a reverberation chamber (RC) was proposed. The RC facility is able to reproduce a  
 2 real environment, where the electromagnetic field is statistically uniform, isotropic and with random

383 polarization [58]. In this way, the sample was excited from all the possible directions (polarization  
384 and incident angle), as a real-life scenario. In order to evaluate the SE, a smaller chamber with an  
385 aperture, called nested chamber, was used. The sample under test (Table 5) was mounted on the  
386 aperture [59,60]. Fig. 5a shows the adopted measurement setup. The outer RC which excites the  
387 material under test had dimensions of  $6 \times 4 \times 2.5 \text{ m}^3$ , whereas the inner chamber of  $1.2 \times 0.9 \times 0.8 \text{ m}^3$ .  
388 Within the outer RC, vertical and horizontal stirrers made of metallic rotating paddles provided the  
389 field mixing. The sample was placed on the aperture (Fig. 5b). In order to have an optimal contact  
390 between the sample edges and the aperture perimeter, avoiding field leakages [61], electromagnetic  
391 gaskets was used (Fig. 5b). Moreover, in order to improve the contact between the sample and the  
392 aperture, a multi-hole frame (Fig. 5c) with screws, pushing the sample towards the underlying  
393 gaskets, was used (Fig. 5d).

394



395

6 **Fig. 5.** a) Measurement set-up: outer RC equipped by vertical and horizontal stirrers, two log-periodic  
7 antennas and nested RC with the aperture on the top; b) aperture of the nested RC where both the  
8 gaskets used to avoid field leakages and the holes, where the multi-hole frame was mounted with  
9 screws to fasten the specimens and to provide a good contact, are visible; c) multi hole frame used to

400 improve the mechanical contact between the sample and the aperture; d) multi hole frame mounted  
401 on the aperture.

402

403 The outer reverberation chamber was fed by a log-periodic antenna (#1) and the resulting energy  
404 exciting the sample was monitored by a second antenna (#2) of the same type (Fig. 5a). The field  
405 inside the nested chamber was picked up by two double ridge antennas, receiving (#3) and  
406 transmitting (#4). A four port Vector Network Analyzer (VNA) was connected to the system to  
407 measure the scattering parameters between the four antennas: (#1) and (#2) for the outer chamber and  
408 (#3) and (#4) for the inner one. The power received was given by  $|S_{ij}|^2$ , where S is the complex  
409 scattering coefficient measured by the VNA, i and j are the receiving and transmitting antennas,  
410 respectively. In this case, the power received inside the outer and inside the inner reverberation  
411 chamber and the power between the outer to inner chamber were  $|S_{21}|^2$ ,  $|S_{43}|^2$  and  $|S_{31}|^2$ , respectively.  
412 In fact, the material exhibited also effective absorption of electromagnetic energy, thus reducing the  
413 quality factor of both reverberation chambers [62]. The SE was evaluated by:

414

$$415 \quad SE = -10 \log \left( \frac{\langle |S_{21}|_{ns}^2 \rangle \langle |S_{41}|_s^2 \rangle \langle |S_{43}|_{ns}^2 \rangle}{\langle |S_{21}|_s^2 \rangle \langle |S_{41}|_{ns}^2 \rangle \langle |S_{43}|_s^2 \rangle} \right) \quad (2)$$

416

417 where  $\langle \cdot \rangle$  is the ensemble averaged over the chamber realizations, the subscripts  $s$  means “the case  
418 with the specimen” and  $ns$  means “the case without the specimen”. A single chamber realization of  
419 the outer RC corresponded at each stirrer position. On the contrary, within the inner chamber, due to  
420 the limited space, there was not a stirrer. In the inner chamber, a bandwidth with a frequency step of  
421 250 kHz was considered, and the frequency stirring [63] was applied by using 400 frequency points,  
422 each of them correspondent to a chamber realisation. The investigated band was from 0.8 to 8.4 GHz,  
423 divided in several sub-bands of 400 MHz, where 1601 frequency points were acquired by the VNA,  
424 sampled by steps of 250 kHz. The stirrers worked in synchronous way; they had the same angle step  
425 and 9 stirrer positions were considered for both, 40 degrees shifted for each position.

426

### 427 **3. Results and discussions**

#### 428 *3.1. Mechanical and microstructural characterisation*

429 The results of the tensile ( $f_{ct}$ ) and compressive strength ( $R_c$ ) of the pastes during the first 28 days of  
430 curing are reported in Table 6.

431 As for regards the  $f_{ct}$  values, all the pastes show the same behaviour, with a gradual increase of tensile  
432 strength during time; only FS 0.25 and FS 0.50 specimens reach approximately the maximum strength  
433 after 7 days of curing. This effect is related to the presence of alkaline salts in the foundry sand [64]  
434 (Table 1), which have operated as quick setting agents, contributing to a faster development of  
435 mechanical strength during the first days after casting.

436 The maximal enhancement of  $f_{ct}$  is registered for the pastes manufactured with the two commercial  
437 fillers since their strengths are 20% higher than REF if prepared with AC and more than 40% if  
438 prepared with GNP at 1.00 wt.%. Gong et al. [65] found that the use of graphene oxide (GO) inside  
439 Portland cement pastes increases the tensile strength more than the 40% when used at 0.03 wt.% on  
440 the binder content. The great strength enhancement provided by the little amount of GO used by Gong  
441 et al. is related to the great capacity of this material to be dispersed in water, being hydrophilic,  
442 compared to graphene nanoplatelets, which conversely is hydrophobic. Instead, the addition of waste  
443 carbon-based fillers (CH and FS) does not produce any effect on the tensile strength of pastes after  
444 28 days of curing, since the results are comparable with those of REF.

445 Concerning compressive strength, the presence of carbonaceous fillers contributes to increase the  $R_c$   
446 values even after 2 days of curing, compared to the REF paste. Moreover, when CH and FS are added,  
447 the values are two and three times higher, respectively. As for tensile strength, in FS pastes this  
8 behaviour is related to the presence of alkaline salts inside this waste carbon-based filler (Table 1)  
9 which act as quick setting agents. In the case of CH paste, this is probably due to the surface area of  
0 CH particles ( $76 \text{ m}^2/\text{g}$ ) that contributes to the growth of hydration products, giving again an  
1 accelerating effect on the hydration kinetics at early ages, as reported by Gupta and Kua [66] for





452 cement-based mixtures. This behaviour was also detected in [67] where carbon-based fillers were  
 453 added in hydraulic lime-based mortars. Furthermore, each addition at each percentage increases the  
 454 final mechanical strength ( $R_c$  at 28 days) compared to the REF paste, except for AC 1.00 one, up to  
 455 45%. This high content of AC decreases the workability of the paste much more than the other fillers,  
 456 due to its very high specific surface area ( $1800 \text{ m}^2/\text{g}$ ), so that additional water was necessary to reach  
 457 a slump flow value comparable to that of the other pastes (Table 3). The additional water has changed  
 458 the w/b ratio from 0.32 to 0.33 (Table 3), leading to a decrease in  $R_c$  after 28 days [68]. The ability  
 459 of nano/micro fillers to increase the mechanical strength of cement-based materials already at early  
 460 ages is known as “filler effect” [69]. Such materials, due to their high specific surface area [4,70],  
 461 work as nucleation sites for C-S-H [71,72], accelerating the degree of hydration and therefore  
 462 increasing the mechanical properties of hardened compounds. Moreover, it is well-known that the  
 463 addition of fillers contributes to the refinement of the paste, lowering the total porosity ( $V_p$ ) of the  
 464 compound and shifting the critical pore radius ( $r_c$ ) to smaller dimensions. Such effect is well visible  
 465 in Table 6, where the REF paste shows a  $V_p$  of 41% whereas all other pastes have a lower total porosity  
 466 value, which reaches the lowest value (36%) when FS is added. This effect is probably due to the best  
 467 dispersion obtained by FS filler because of the small and spherical shape of its particles (Fig. 1d).  
 468 Moreover, all the manufactured pastes are characterised by  $r_c$  smaller than the REF one, confirming  
 469 the ability of all carbon-based fillers to refine the porosity of the matrix.

471 **Table 6.** Tensile strength ( $f_{ct}$ ), compressive strength ( $R_c$ ), total porosity ( $V_p$ ) and critical pore radius  
 472 ( $r_c$ ) of pastes.

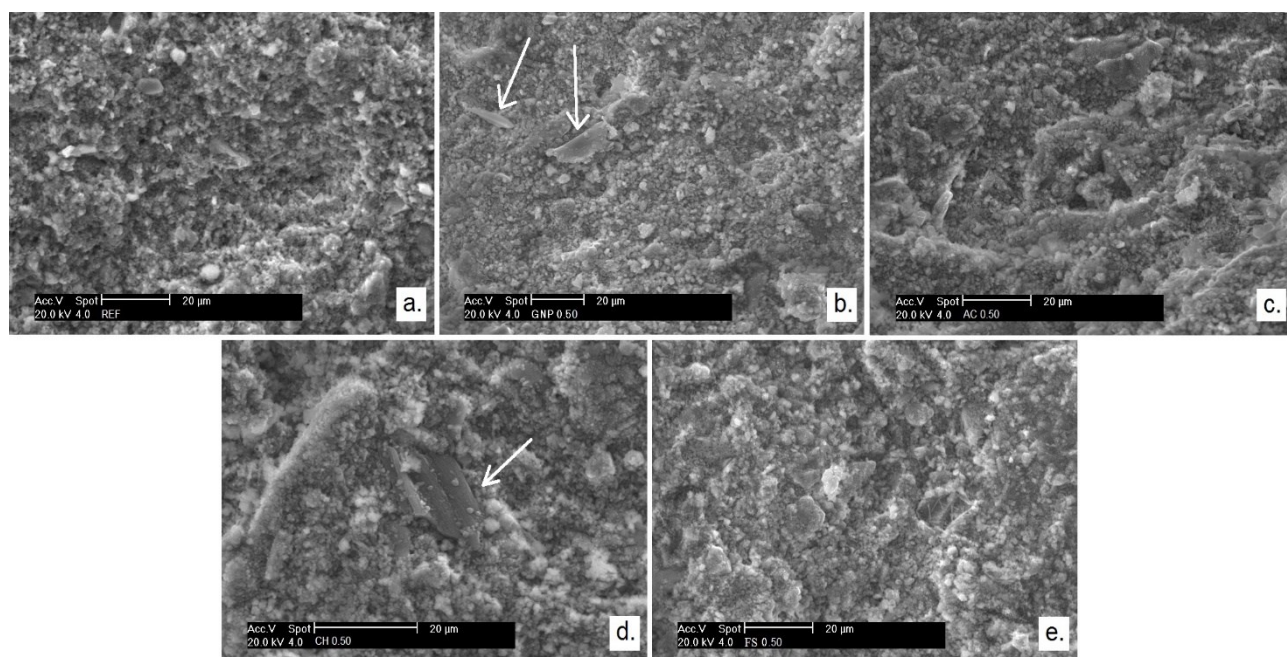
Mixtures	$f_{ct}$ (MPa)			$R_c$ (MPa)			$V_p$ (%)	$r_c$ ( $\mu\text{m}$ )
	2 days	7 days	28 days	2 days	7 days	28 days		
REF	0.20 ± 0.01	0.56 ± 0.00	0.82 ± 0.01	1.2 ± 0.0	4.2 ± 0.1	10.8 ± 0.3	41	0.116
GNP 0.25	0.30 ± 0.03	0.50 ± 0.04	0.92 ± 0.01	1.9 ± 0.0	4.8 ± 0.1	13.0 ± 0.5	37	0.082
GNP 0.50	0.30 ± 0.01	0.65 ± 0.00	0.88 ± 0.01	2.0 ± 0.1	3.5 ± 0.2	13.8 ± 0.1	39	0.103
GNP 1.00	0.40 ± 0.01	0.66 ± 0.01	1.17 ± 0.05	2.3 ± 0.2	3.7 ± 0.0	13.5 ± 0.1	39	0.104
AC 0.25	0.30 ± 0.03	0.48 ± 0.01	0.99 ± 0.00	1.2 ± 0.3	4.4 ± 0.0	12.8 ± 0.0	38	0.093

AC 0.50	0.30 ± 0.03	0.60 ± 0.01	0.97 ± 0.01	1.8 ± 0.0	4.3 ± 0.1	13.3 ± 0.1	38	0.096
AC 1.00	0.40 ± 0.01	0.58 ± 0.00	0.99 ± 0.01	1.7 ± 0.1	4.4 ± 0.1	11.1 ± 0.1	39	0.096
CH 0.25	0.34 ± 0.01	0.56 ± 0.03	0.69 ± 0.01	2.6 ± 0.1	4.2 ± 0.0	12.7 ± 0.2	38	0.111
CH 0.50	0.39 ± 0.00	0.47 ± 0.01	0.82 ± 0.02	2.7 ± 0.1	4.3 ± 0.3	12.1 ± 0.1	40	0.111
CH 1.00	0.39 ± 0.01	0.59 ± 0.03	0.82 ± 0.01	2.8 ± 0.0	5.1 ± 0.4	13.6 ± 0.1	39	0.110
FS 0.25	0.51 ± 0.01	0.85 ± 0.03	0.88 ± 0.03	3.7 ± 0.1	6.4 ± 0.2	15.8 ± 0.3	37	0.086
FS 0.50	0.57 ± 0.01	0.97 ± 0.04	0.82 ± 0.03	3.5 ± 0.2	7.5 ± 0.4	13.3 ± 0.0	36	0.084
FS 1.00	0.43 ± 0.00	0.58 ± 0.01	0.79 ± 0.01	3.0 ± 0.1	5.2 ± 0.1	13.1 ± 0.1	36	0.099

473

474 The SEM images of the REF paste and those manufactured with carbon-based fillers at 0.50 wt.% are  
 475 given in Fig. 7. In AC 0.50 and FS 0.50 specimens (Figs. 7c and 7e), the presence of the carbonaceous  
 476 addition is not visible, whereas in GNP 0.50 two agglomerates of graphene nanoplatelets partially  
 477 embedded in the matrix can be noticed in the upper left side (Fig. 7b), confirming the higher  
 478 difficulties in dispersing the GNP with respect to the other fillers. In CH 0.50 specimen, the presence  
 479 of one particle of char perfectly adhered to the paste is visible in the middle area of Fig. 7d. The  
 480 surface of CH particle is covered by the precipitation of hydration products, confirming again the  
 481 capacity of CH to increase their growth [66].

482



3

484 **Fig. 7.** SEM of pastes: a. REF; b. GNP 0.50; c. AC 050; d. CH 0.50; e. FS 0.50. Arrows indicate the  
485 carbonaceous particles.

486

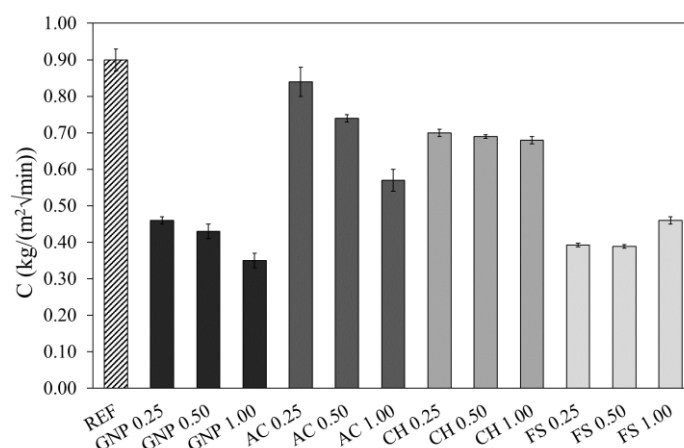
### 487 3.2. Capillary water absorption

488 As for regards the water absorption coefficient ( $C$ ) (Fig. 8), carbonaceous fillers have a great influence  
489 in decreasing the water uptake of pastes at short periods of contact with water (90 min). When GNP  
490 and FS fillers are used,  $C$  coefficient reaches values lower than half of that of REF. In general,  
491 increasing carbon-based fillers content, the water suction decreases, especially for pastes prepared  
492 with the two commercial fillers, since both AC [73,74] and GNP [75–77] are hydrophobic materials.  
493 This behaviour is less evident for pastes which contain CH, since their  $C$  values remain always around  
494 76% of REF: this effect is related to their critical pore radii which are bigger than those of the pastes  
495 manufactured with other fillers (Table 6). The results confirm that the saturation of the capillary pores  
496 with higher dimensions occurs faster than for the smaller ones [78].

497 On the other hand,  $C$  value has a reversal trend when FS is used, seeing that it increases with the  
498 amount of this filler, with absorption values equal to 43% and 54% of REF when 0.25% and 1.00%  
499 of FS are added, respectively. The increased content of FS increases also the presence of clay  
500 impurities [64,79]; it is well-known that clay is hydrophilic and thus it is much prone to water  
501 absorption [68]. However, FS specimens show very low  $C$  coefficients thanks to their low total  
502 porosities and small critical pore radii  $r_c$  (Table 6).

503





504

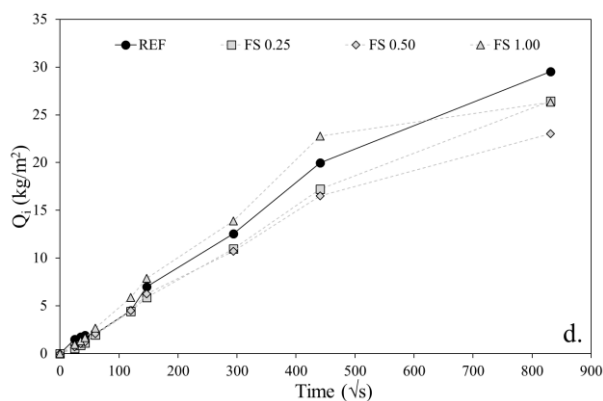
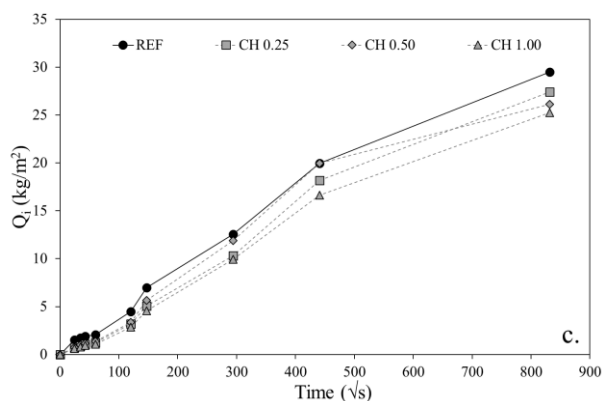
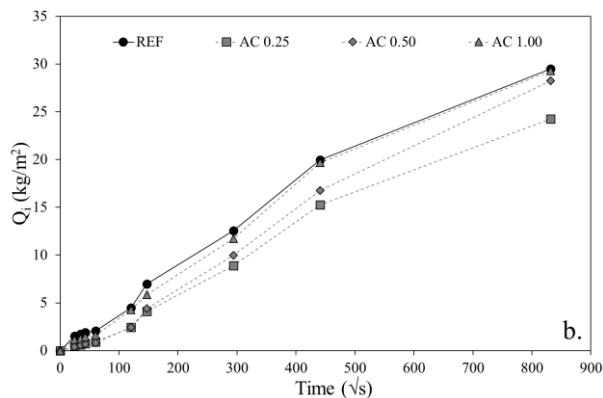
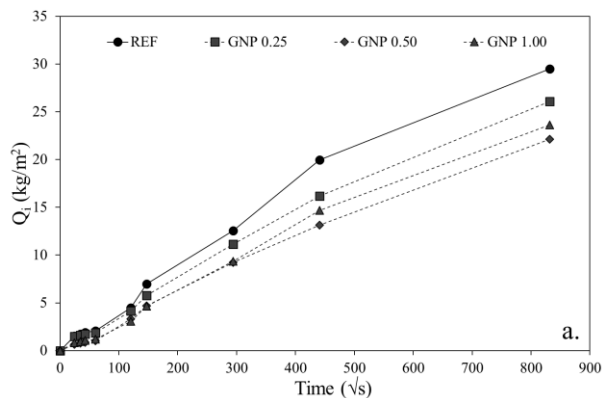
505 **Fig. 8.** Water absorption coefficient ( $C$ ) of pastes after 28 days of curing.

506

507 The water absorbed per unit area ( $Q_i$ ) by pastes after 28 days of curing is reported in Fig. 9. Also for  
 508 a long time of contact with water (8 days), all specimens containing carbon-based fillers show a lower  
 509 absorption compared to REF. In particular, the lowest absorptions are registered for GNP pastes (Fig.  
 510 9a), confirming again the hydrophobic nature of GNP; GNP filler, acting as a barrier against the rise  
 511 of capillary water, increases the winding of the water path [48]. Also the pastes containing FS exhibit  
 512 very low water absorptions in time (Fig. 9d) thanks to their lowest total porosity (Table 6). In these  
 513 cases, the lowest absorptions are obtained by the specimens manufactured with 0.50 wt.% of filler.  
 514 For FS 0.50 paste this is due to the smallest dimensions of the critical pore radius (Table 6); for the  
 515 GNP 0.50 paste this is due to the hydrophobicity of graphene particles, since neither the total porosity  
 516 nor the critical pore radius of GNP pastes are the smallest (Table 6).

517 The  $Q_i$  values of the pastes manufactured with AC (Fig. 9b) show an opposite trend compared to the  
 518  $C$  coefficient (Fig. 8). In fact, whereas the  $C$  coefficient increases with the AC content, the absorption  
 519 decreases. This effect is related to the AC behaviour: AC is hydrophobic only at early ages thanks to  
 0 its non-polar surface characteristics [80], whereas it becomes hydrophilic for long contact time with  
 1 water [73].

2



523

524

525 **Fig. 9.** Water absorbed per unit area ( $Q_i$ ) of pastes after 28 days of curing. In each figure, the  
 526 continuous line represents the REF paste.

527

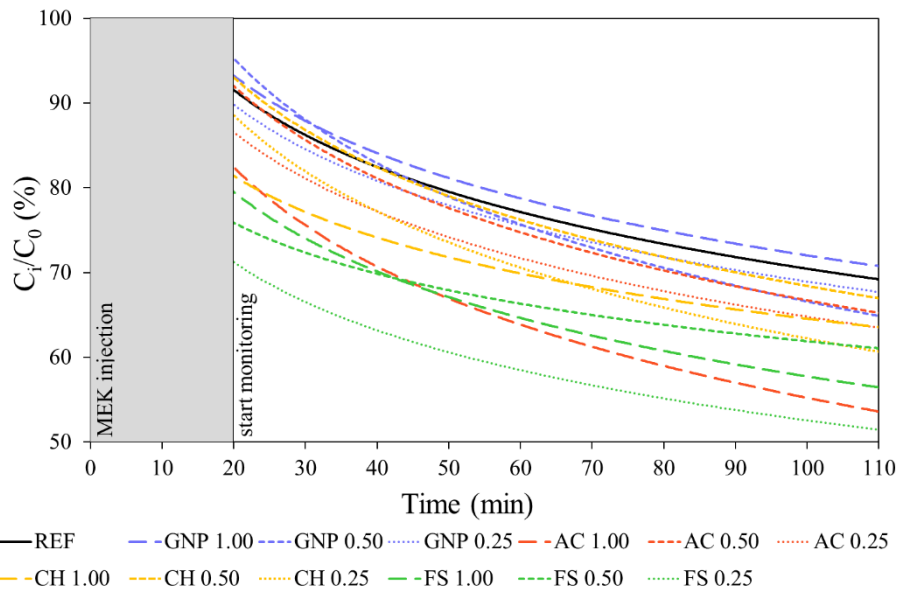
528 *3.3. Depolluting tests*

529 *3.3.1. In batch test*

530 The depolluting capacity of the pastes under dark condition is displayed in Fig. 10, where the residual  
 531 percentage of MEK inside the box is plotted against time. The trendline starts at 20 minutes because  
 532 this is the time necessary for vaporising MEK completely.

533





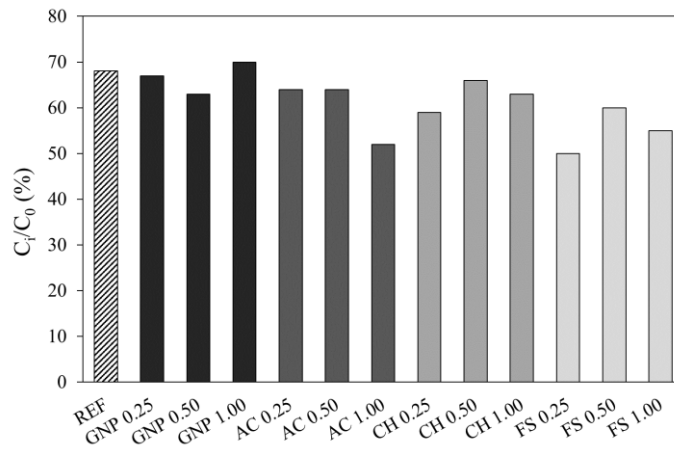
534

535 **Fig. 10.** Residual percentage of MEK inside the box during the in batch test carried out on pastes.

536

537 To better analyse and compare the results, in Fig. 11 the residual percentage concentration of MEK  
 538 ( $C_i/C_0$ ) inside the box after 110 min of test under dark condition is also reported.

539



540

541 **Fig. 11.** Residual percentage of MEK inside the box during the in batch test on pastes after 110 min.

542

3 Fig. 10 and Fig. 11 show that under dark condition the REF paste adsorbs approximately 30% of  
 4 MEK at the end of test. Only pastes manufactured with some carbonaceous fillers improve this  
 5 depolluting capacity. In particular, when GNP is added the depolluting efficiency remains around  
 6 30%. AC, instead, when added at 1.00 wt.% of lime, increases the efficiency to 50%. Thanks to the



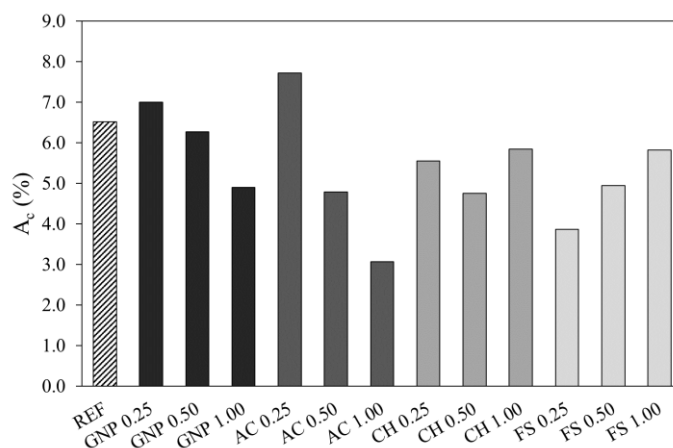
547 great ability of AC to reduce air pollutants by adsorption [81] because of its high specific surface area  
548 (1800 m<sup>2</sup>/g), a minimum amount of 1.00 wt.%, as in this case, is enough to obtain a significant effect.  
549 Referring to carbon waste fillers, the CH pastes show a poor effect on MEK removal, this can be  
550 ascribed to its surface area which is not so high (76 m<sup>2</sup>/g). Even if CH is considered a potential  
551 substitute of AC for VOCs removal [34], in this case it seems not compatible for adsorbing MEK. FS  
552 appears the most effective filler to increase the depolluting capacity of pastes given that, by varying  
553 its content, residual concentrations of MEK around 40 – 50% can be achieved, even if its specific  
554 surface area (341 m<sup>2</sup>/g) is lower than AC.

555

### 556 3.3.2. Flow test

557 The photocatalytic efficiency of the pastes tested in terms of NO<sub>x</sub> abatement under UVA radiation is  
558 shown in Fig. 12.

559



560

561 **Fig. 12.** Photocatalytic efficiency under UVA radiation of pastes (NO<sub>x</sub> abatement).

562

3 Both commercial and waste carbonaceous fillers do not modify the NO<sub>x</sub> abatement of the REF paste  
4 which is too low (6.5%) to be considered as a photocatalytic behaviour.

5 For the above-mentioned reason, it was decided to test some selected pastes with the addition of nano-  
6 TiO<sub>2</sub>, that is known to be an efficient photocatalytic agent [6], in order to evaluate if the carbon-based

567 fillers could affect the photocatalytic activity of TiO<sub>2</sub> improving the first stage of photoactivity  
568 (adsorption of pollutants). In fact, carbonaceous fillers could interact with the photocatalyst; keeping  
569 the surface chemistry unchanged, the increase of the specific surface area can create a high number  
570 of active sites and e<sup>-</sup>-h<sup>+</sup> pairs and high concentration of pollutants on the photocatalyst can be  
571 expected [82]. For this reason, some pastes were manufactured using carbonaceous fillers at 0.50  
572 wt.% and TiO<sub>2</sub> at 1.00 wt.% on hydraulic lime (Table 4).

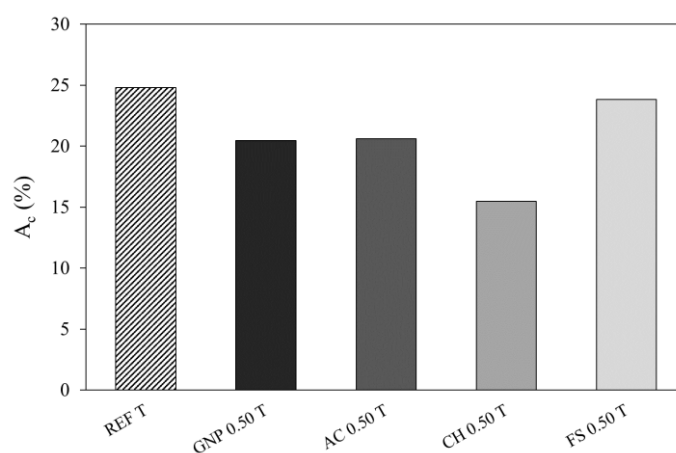
573 Results of the photocatalytic efficiency of the pastes with TiO<sub>2</sub> addition are reported in Fig. 13. When  
574 TiO<sub>2</sub> is added to the paste (REF T), the NO<sub>x</sub> abatement reaches values of 25%, four times higher than  
575 that of the same paste without TiO<sub>2</sub> (REF specimen, Fig. 12). **This result was also reported by some**  
576 **of the present authors in a recent paper [83], where the replacement of hydraulic lime with TiO<sub>2</sub> at 5**  
577 **wt.% in a plain mortar contributes to enhance the photocatalytic efficiency from 5% to 35%. In**  
578 general, also using carbonaceous fillers, all the pastes with TiO<sub>2</sub> show a great enhancement of the  
579 photocatalytic action. In particular, GNP 0.50 T and AC 0.50 T show an  $A_c$  value around 20%, which  
580 are four and three times higher than that of GNP 0.50 and AC 0.50, respectively (Fig. 12). As for  
581 regards the waste carbon-based additions, the lowest NO<sub>x</sub> abatement is found for CH 0.50 T with an  
582  $A_c$  value of 15%, which is three times higher than that registered for CH 0.50 specimen (Fig. 12). On  
583 the contrary, the specimen manufactured with TiO<sub>2</sub> and foundry sand (FS 0.50 T) shows the same  
584 photocatalytic efficiency of REF T, five times higher than that of the same paste without  
585 photocatalytic agent (Fig. 12).

586 Observing the results of Fig. 12 and Fig. 13, it is evident that the addition of a photocatalytic agent is  
587 necessary to obtain the photocatalytic abatement of NO<sub>x</sub> under UVA irradiation. The results  
588 demonstrate that the addition of carbonaceous fillers, without specific treatments, is not able to  
9 increase the photocatalytic behaviour of TiO<sub>2</sub>. For example, with GNP this effect can be only  
0 achieved by using a functionalisation method [84], like hydrothermal [85] or sol-gel [86] treatments.  
1 Moreover, the addition of carbonaceous fillers always worsens the depollution behaviour of pastes  
2 compared to the reference one: only in the case of FS, the paste shows a result comparable to the



593 reference one, whereas the photocatalytic efficiency decreases by 20% in the case of GNP and AC  
 594 addition, and even 40% in the case of CH addition. This effect could be related to the colouration that  
 595 the specimens acquire because of the presence of the fillers, since their black colour has darkened the  
 596 paste (Fig. 14). Only the one manufactured with FS shows a colour similar to that of REF T (Fig. 14a  
 597 and 14c). It is reported that the addition of pigments, that provide a significant coloration on finishing  
 598 products, can induce a moderate decrease of the photocatalytic activity in terms of NO<sub>x</sub> abatement  
 599 [87,88]. This result was also reported in [83], where the use of activated carbon in place of natural  
 600 sand in TiO<sub>2</sub>-rich hydraulic lime based mortars resulted in a decrease of the photocatalytic efficiency  
 601 of about 40%, because the reduced reflectance of radiation of the darkened substrate has lowered the  
 602 photocatalytic properties of the mortar [89].

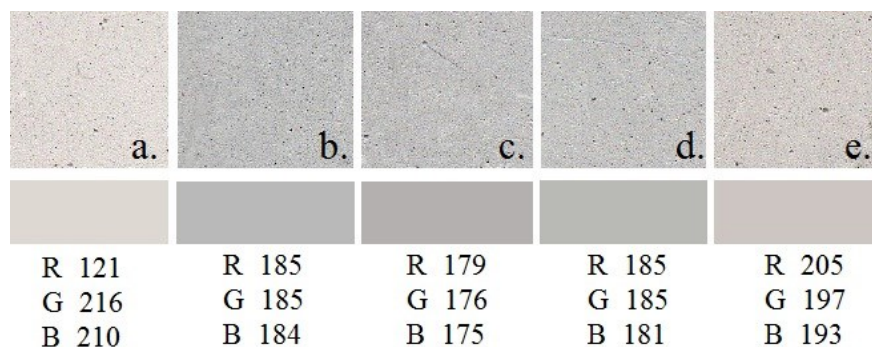
603



604

605 **Fig. 13.** Photocatalytic efficiency under UVA radiation of pastes (NO<sub>x</sub> abatement) with TiO<sub>2</sub> addition.

606



7

608 **Fig. 14.** Scan images of the specimens' surface (up) and average RGB value measured in five different  
609 points (down): a. REF T, b. GNP 0.50 T, c. AC 0.50 T, d. CH 0.50 T, e. FS 0.50 T.

610

### 611 3.4. Electromagnetic characterization

#### 612 3.4.1. Electrical resistivity

613 The DC electrical resistivity ( $\rho$ ) measurements conducted on the paste specimens at 7, 14, 21 and 28  
614 days of curing are displayed in Fig. 15.

615 After the first week (Fig. 15a), the REF paste registers an electrical resistivity of 170  $\Omega\cdot\text{cm}$ . All the  
616 other pastes show similar  $\rho$  values ranging from 190 to 170  $\Omega\cdot\text{cm}$ , unless that prepared with the FS  
617 filler, which shows a higher electrical resistivity. Moving towards 0.25 to 0.50 and 1.00 percentages  
618 of FS, the electrical resistivity decreases with values equal to 790, 360 and 210  $\Omega\cdot\text{cm}$ , respectively.

619 However, in these pastes the electrical resistivity decreases by increasing FS addition, as reported in  
620 literature for GNP [2], carbon black [49,54], carbon coke [53] and graphite [14] additions.

621 After 14 days, the electrical resistivity of pastes increases of one order of magnitude (Fig. 15b). The  
622  $\rho$  measured in the REF paste is about 3400  $\Omega\cdot\text{cm}$ , whereas all the other specimens with carbon-based  
623 additions show a lower electrical resistivity. In general, a clear trend related to the different additions  
624 of the same filler and electrical resistivity is not visible; in fact, only those with FS maintain the trend  
625 observed at 7 days of curing.

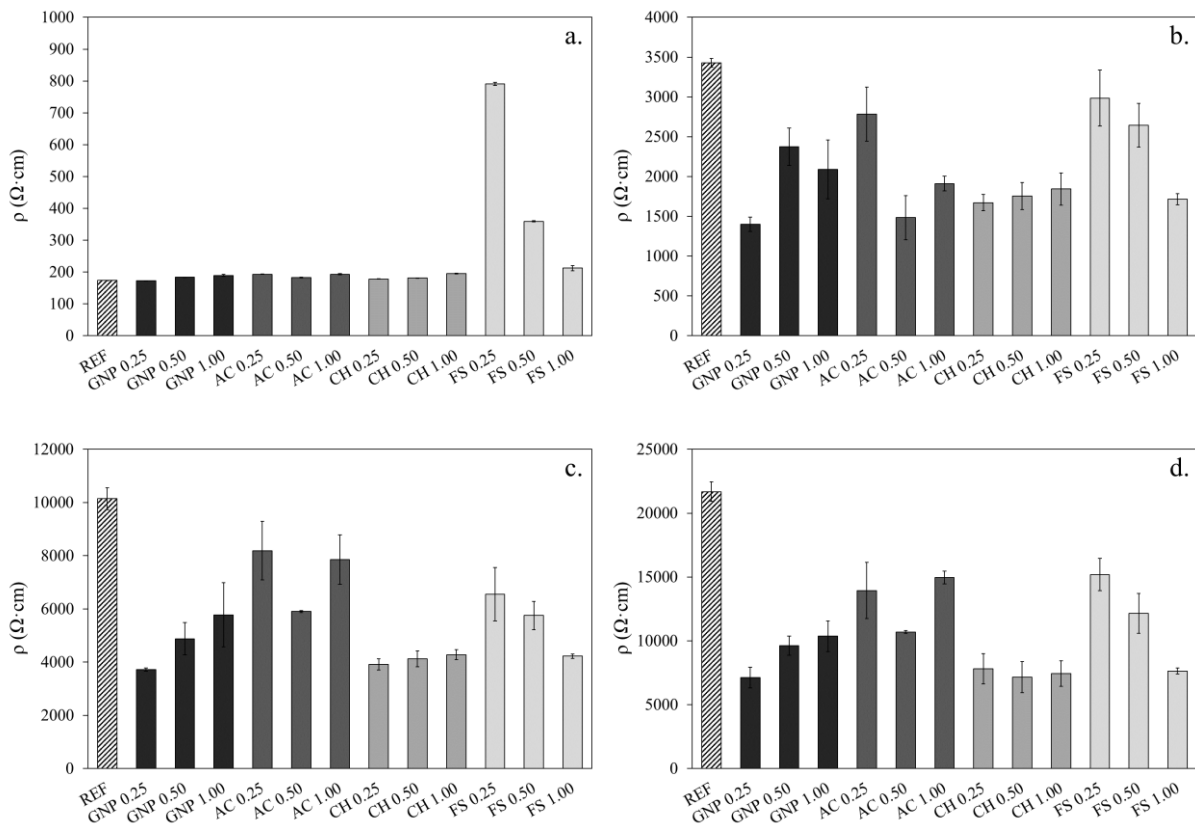
626 After 21 days from casting (Fig. 15c),  $\rho$  values continue to increase, especially for REF paste,  
627 achieving approximately 10000  $\Omega\cdot\text{cm}$ . Also at this curing period, all pastes containing carbonaceous  
628 fillers assume lower values of  $\rho$  than REF, even if those manufactured with GNP show an opposite  
629 trend compared to that reported in literature since the higher the amount of the carbon-based fillers,  
0 the higher the resistivity. This effect could be related to the agglomeration of GNP particles  
1 [28,90,91], as observed in Fig. 7. It is reported that the decrease of electrical resistivity with the  
2 increase of carbon-based fillers dosage is obtained only when the amount remains under the  
3 percolation threshold and the particles are well dispersed or, above this value, a further decrease of



634 electrical resistivity occurs only if fillers segregate along the continuous conduction paths [92]. The  
635 percolation threshold is the volume fraction above which the adjacent admixture units, whether fibres  
636 or particles, touch the one to another forming a continuous conduction path [54]. For GNP, the  
637 percolation threshold has been found to be between 10 and 15 wt.% by cement [2], much higher than  
638 the amount of GNP used in the present paper. When AC is used,  $\rho$  shows a decrease from 0.25 to  
639 0.50 wt.% AC addition and then  $\rho$  increases at 1.00 wt.% addition. It is possible that also for the AC  
640 paste, the increase of  $\rho$  values is due to the agglomeration of particles which have discontinued the  
641 available current paths. As for regards the waste carbon fillers, the electrical resistivity of CH  
642 specimens, regardless the addition amount, is approximately 4000  $\Omega \cdot \text{cm}$  which is 60% lower than  
643 REF, whereas FS specimens continue to maintain the same trend registered at previous ages.  
644 After 28 days (Fig. 15d) the electrical resistivity increases again and, for REF paste it doubles the  
645 value registered at 21 days reaching 22000  $\Omega \cdot \text{cm}$ . For the specimens with carbonaceous additions,  
646 the trend measured at 21 days is confirmed. In general, at 21 and 28 days of curing, the lowest  $\rho$   
647 values (approximately 65% lower than REF) are found for GNP 0.25, for all specimens manufactured  
648 with CH, and for FS 1.00 paste.  
649 The good electrical properties given by carbon-based addition are related to both their carbon content,  
650 which is high especially for GNP and AC, and to their good dispersion within the matrix, as in the  
651 case of waste CH and FS fillers.

652





653

654

655 **Fig. 15.** DC electrical resistivity ( $\rho$ ) of pastes after: a. 7, b. 14, c. 21, d. 28 days of curing.

656

### 657 3.4.1. Electromagnetic shielding property

658 Generally, the electromagnetic shielding property increases with electrical conductivity. Since the  
 659 lowest electrical resistivity values were found in pastes with waste carbonaceous fillers at the highest  
 660 percentages (1.00 wt.%) and commercial fillers at 0.50 wt.%, the SE was determined only for these  
 661 mixes. However, SE was measured not on pastes but on mortars (Table 5) since a perfect adhesion  
 662 between the specimens and the mould used for the test shall be ensured and mortars shrink less than  
 663 pastes.

664 The obtained results are given in Fig. 16. **It should be stressed that in literature, there is no paper**  
 5 **considering the behaviour of carbonaceous additions on the SE of lime-based mortars.** In general, the  
 6 SE of the present mortars is similar to that of cement-based mixes [33], as shown also by Samková  
 7 et al. [93] who tested plasters manufactured with different binders and found that the SE of plain  
 8 cement- and lime-based pastes was **comparable**. All mortars with carbonaceous additions register a



669 higher, or at least similar, SE compared to that of M REF; in particular, M GNP 0.50 mortar always  
670 shows a SE 1 or 2 dB higher than the reference one. Only M AC 0.50 mortar shows a lower SE than  
671 M REF at each investigated frequency value.

672 In order to analyse the obtained results in detail, Fig. 17 shows figures enlarged at 2 – 3 GHz, 4 – 5  
673 GHz and 6 – 7 GHz, since in these frequency ranges the differences between mortars are more visible.

674 These frequencies are mostly familiar with wireless communication systems. Frequencies of 2.1 GHz  
675 and 2.6 GHz are used for telecommunication mobile phones, Universal Mobile Telecommunications  
676 System (UMTS) and fourth generation Long Term Evolution (4G-LTE), respectively. Moreover, 2.45

677 GHz for the Bluetooth standard, whereas 2.4 GHz and 5 GHz are used for wireless networks. The  
678 frequency of 7 GHz is dedicated for point-to-point narrow band systems, as Plesiochronous Digital  
679 Hierarchy/Synchronous Digital Hierarchy (PDH/SDH). In these frequency ranges, M GNP 0.50

680 increases SE of about 30% compared to M REF. Also the carbon-based waste fillers enhance the SE  
681 at 2 – 3 GHz, 4 – 5 GHz and 6 – 7 GHz compared to the M REF mortar, even though the best  
682 improvement is around 6% for M CH 1.00 mortar. These results confirm that the fillers giving the

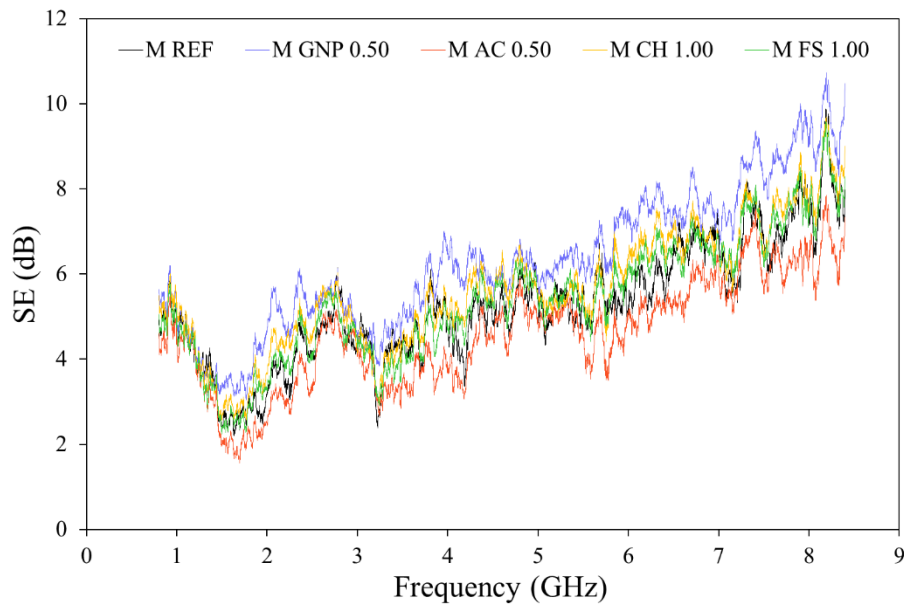
683 lowest electrical resistivity to the pastes are also those giving the highest SE values. In general, the  
684 high specific surface area, the high chemical stability and the high conductivity of graphene have

685 been reported to be the key parameters for its good EM wave absorption properties [94,95]. It has  
686 been found that a low dosage of GNP equal to 0.1 wt.% is able to increase the electromagnetic wave  
687 absorption of cement-based materials [94]. Therefore, even if GNP is surely the most effective filler

688 for enhancing the electromagnetic shielding properties of binder-based materials, in this study also  
689 priceless waste carbonaceous fillers can improve this property [33]. The increased electromagnetic  
690 SE of the mortar containing CH filler is due to its very good dispersion, which has formed a connected

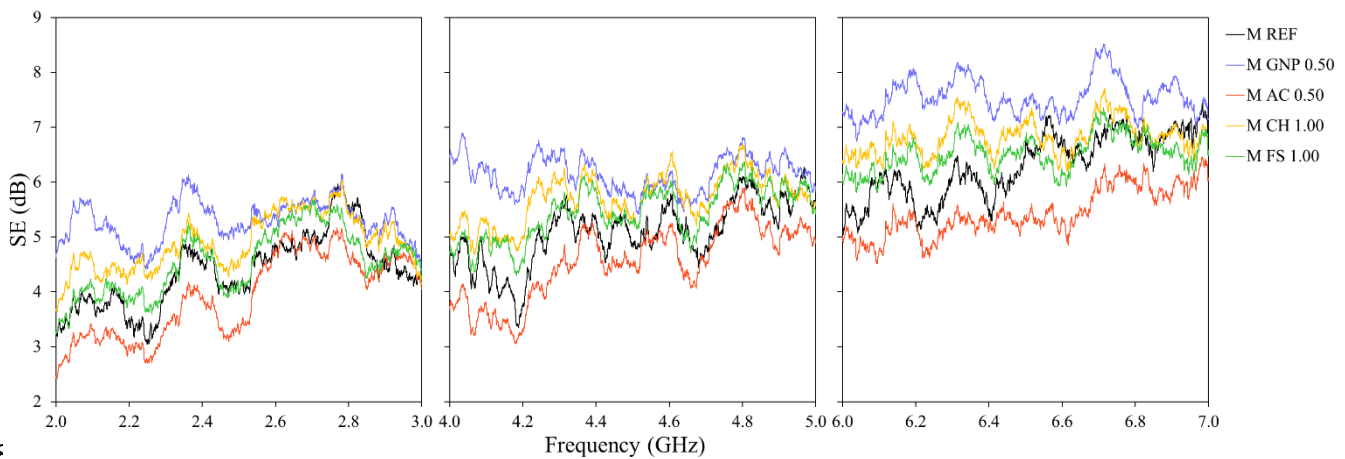
1 and conductive network able to enhance the electrical conductivity of the material and to the enhanced  
2 interfacial polarization of CH, as found by Mahmood et al. [96] who obtained the best SE by using  
3 carbonized cotton stalk in mortars at 0.5 wt.% by cement.  
4





695  
696 **Fig. 16.** Shielding effectiveness (SE) of mortars after 21 days of curing.

697



698  
699 **Fig. 17.** Shielding effectiveness (SE) of mortars after 21 days of curing in the ranges of frequencies  
700 between 2 – 3, 4 – 5 and 6 – 7 GHz.

701

#### 702 **4. Conclusions**

703 The use of commercial and waste carbon-based micro-fillers was investigated in order to improve the  
704 mechanical, durability, depolluting, electrical and electromagnetic properties of hydraulic lime-based  
705 pastes and mortars. As commercial fillers, graphene nanoplatelets (GNP) and powdered activated  
706 carbon (AC) were used. As priceless wastes, a char (CH) obtained by the gasification process of

707 biomasses and the finest fraction of a used foundry sand (FS) were chosen. Fillers were added at 0.25,  
708 0.50 and 1.00 % on lime weight.

709 The obtained results suggest the following conclusions:

- 710 • The addition of carbonaceous fillers, regardless of their nature and amount, is essential to  
711 reduce the total porosity and the critical pore radius of pastes. The resulting “filler effect”  
712 enhances the tensile strength of 40% and 20% when GNP and AC are added at 1.00 wt.% on  
713 the lime, respectively. Particularly the compressive strength is increased for all the type of  
714 additions, both commercial and waste up to 45%.
- 715 • The reduced porosity and the smaller critical pore radius lower the capillary water absorption  
716 of pastes at each percentage and type of carbonaceous addition, both at short and long time  
717 of contact with water. At early ages, the capillary water absorption is decreased more than  
718 50% with GNP and FS.
- 719 • The depollution capacity of the pastes, in terms of MEK adsorption, enhances mostly by the  
720 addition of AC at 1.00 wt.%. However, both the waste fillers, at all percentages, show very  
721 good adsorption capacity, even equal to 50% when FS is added.
- 722 • No one of the carbonaceous fillers is effective to produce a photocatalytic activity to the  
723 pastes when a photocatalytic agent is absent. Under UVA radiation and in the presence of  
724 TiO<sub>2</sub>, the carbonaceous fillers even decrease the photocatalytic behaviour because of the  
725 darkening of the paste.
- 726 • Both the commercial and waste carbon-based fillers decrease the electrical resistivity of the  
727 lime pastes; in particular, the use of CH decreases the electrical resistivity up to 65% as for  
728 GNP at 0.25 wt.% and FS at 1.00 wt.%. This finding could be interesting for the development  
9 of the so called “self-sensing” mortars/concretes.
- 0 • The highest EMI SE have been found for mortars containing GNP and CH; in particular, the  
1 SE is enhanced by 6% in case of CH and even by 30% in case of GNP.



732 For the above-described results, it can be affirmed that addition of cheap waste carbon-based fillers,  
733 such as gasification char and the finest fraction of a used foundry sand, can be a better alternative in  
734 terms of cost/efficiency to more expensive and less sustainable commercial carbon based fillers, as  
735 graphene nanoplatelets and activated carbon, to improve several properties of lime-based  
736 pastes/mortars. In fact, the price of GNP is approximately 370 €/kg and the price of AC is around 260  
737 €/kg, whereas CH and FS, being wastes, have no commercial value. In particular, in the present work  
738 it has been found that waste carbonaceous fillers are able to increase the mechanical strength, the  
739 durability in terms of capillary water absorption, the depolluting capacity in terms of VOCs  
740 adsorption, the electrical conductivity and, even if slightly, the shielding effectiveness of lime-based  
741 pastes/mortars that can be used for indoor renders and panels.

742

#### 743 **Acknowledgements**

744 The authors wish to thank Pentachem S.r.l. for the graphene nanoplatelets, Cabot Norit Nederland  
745 B.V. for the activated carbon, LA.BO S.r.l. for the used foundry sand kindly offered for this work,  
746 and DIASEN S.r.l. to have co-financed a Ph.D. fellowship on "Carbon based fillers for the  
747 development of innovative multifunctional mortars and plasters" (Eng. Alberto Belli).

748

#### 749 **References**

- 750 [1] A. Mohammed, J.G. Sanjayan, W.H. Duan, A. Nazari, Incorporating graphene oxide in  
751 cement composites: A study of transport properties, *Constr. Build. Mater.* 84 (2015) 341–  
752 347. doi:10.1016/j.conbuildmat.2015.01.083.
- 753 [2] J.-L. Le, H. Du, S.D. Pang, Use of 2D Graphene Nanoplatelets (GNP) in cement composites  
4 for structural health evaluation, *Compos. Part B Eng.* 67 (2014) 555–563.  
5 doi:10.1016/j.compositesb.2014.08.005.
- 6 [3] D.D.L. Chung, Carbon materials for structural self-sensing, electromagnetic shielding and  
7 thermal interfacing, *Carbon N. Y.* 50 (2012) 3342–3353. doi:10.1016/j.carbon.2012.01.031.



- 758 [4] S. Chuah, Z. Pan, J.G. Sanjayan, C.M. Wang, W.H. Duan, Nano reinforced cement and  
759 concrete composites and new perspective from graphene oxide, *Constr. Build. Mater.* 73  
760 (2014) 113–124. doi:10.1016/j.conbuildmat.2014.09.040.
- 761 [5] B. Han, S. Sun, S. Ding, L. Zhang, X. Yu, J. Ou, Review of nanocarbon-engineered  
762 multifunctional cementitious composites, *Compos. Part A Appl. Sci. Manuf.* 70 (2015) 69–  
763 81. doi:10.1016/j.compositesa.2014.12.002.
- 764 [6] F. Pacheco-Torgal, S. Jalali, Nanotechnology: Advantages and drawbacks in the field of  
765 construction and building materials, *Constr. Build. Mater.* 25 (2011) 582–590.  
766 doi:10.1016/j.conbuildmat.2010.07.009.
- 767 [7] D. Micheli, R. Pastore, A. Vricella, R.B. Morles, M. Marchetti, A. Delfini, F. Moglie, V.  
768 Mariani Primiani, Electromagnetic characterization and shielding effectiveness of concrete  
769 composite reinforced with carbon nanotubes in the mobile phones frequency band, *Mater.*  
770 *Sci. Eng. B.* 188 (2014) 119–129. doi:10.1016/j.mseb.2014.07.001.
- 771 [8] C. Giosuè, M. Pierpaoli, A. Mobili, M.L. Ruello, F. Tittarelli, Influence of Binders and  
772 Lightweight Aggregates on the Properties of Cementitious Mortars: From Traditional  
773 Requirements to Indoor Air Quality Improvement, *Materials (Basel)*. 10 (2017) 978.  
774 doi:10.3390/ma10080978.
- 775 [9] S.E. Frey, H. Destailats, S. Cohn, S. Ahrentzen, M.P. Fraser, The effects of an energy  
776 efficiency retrofit on indoor air quality, *Indoor Air*. 25 (2015) 210–219.  
777 doi:10.1111/ina.12134.
- 778 [10] C. Beall, E. Delzell, P. Cole, I. Brill, Brain Tumors among Electronics Industry Workers,  
779 *Epidemiology*. 7 (1996) 125–130.  
0 [http://journals.lww.com/epidem/abstract/1996/03000/brain\\_tumors\\_among\\_electronics\\_indu](http://journals.lww.com/epidem/abstract/1996/03000/brain_tumors_among_electronics_industry_workers.4.aspx)  
1 [stry\\_workers.4.aspx](http://journals.lww.com/epidem/abstract/1996/03000/brain_tumors_among_electronics_industry_workers.4.aspx).
- 2 [11] K.W. Andrews, D.A. Savitz, Accuracy of industry and occupation on death certificates of  
3 electric utility workers: Implications for epidemiologic studies of magnetic fields and cancer,



- 784 Bioelectromagnetics. 20 (1999) 512–518. doi:10.1002/(SICI)1521-  
785 186X(199912)20:8<512::AID-BEM5>3.0.CO;2-M.
- 786 [12] H. Guan, S. Liu, Y. Duan, J. Cheng, Cement based electromagnetic shielding and absorbing  
787 building materials, *Cem. Concr. Compos.* 28 (2006) 468–474.  
788 doi:10.1016/j.cemconcomp.2005.12.004.
- 789 [13] J. Chen, D. Zhao, H. Ge, J. Wang, Graphene oxide-deposited carbon fiber/cement composites  
790 for electromagnetic interference shielding application, *Constr. Build. Mater.* 84 (2015) 66–  
791 72. doi:10.1016/j.conbuildmat.2015.03.050.
- 792 [14] J. Cao, D.D.L. Chung, Colloidal graphite as an admixture in cement and as a coating on  
793 cement for electromagnetic interference shielding, *Cem. Concr. Res.* 33 (2003) 1737–1740.  
794 doi:10.1016/S0008-8846(03)00152-2.
- 795 [15] L. Zhong, F. Haghghat, Photocatalytic air cleaners and materials technologies - Abilities and  
796 limitations, *Build. Environ.* 91 (2015) 191–203. doi:10.1016/j.buildenv.2015.01.033.
- 797 [16] C. Giosuè, A. Belli, A. Mobili, B. Citterio, F. Biavasco, M.L. Ruello, F. Tittarelli, Improving  
798 the Impact of Commercial Paint on Indoor Air Quality by Using Highly Porous Fillers,  
799 *Buildings.* 7 (2017) 110. doi:10.3390/buildings7040110.
- 800 [17] S. Lorencik, Q.L. Yu, H.J.H. Brouwers, Photocatalytic coating for indoor air purification:  
801 Synergetic effect of photocatalyst dosage and silica modification, *Chem. Eng. J.* 306 (2016)  
802 942–952. doi:10.1016/j.cej.2016.07.093.
- 803 [18] D.D.L. Chung, Electromagnetic interference shielding effectiveness of carbon materials,  
804 *Carbon N. Y.* 39 (2001) 279–285. doi:10.1016/S0008-6223(00)00184-6.
- 805 [19] M.-H. Lai, R.Q. Chu, H.-C. Huang, S.-H. Shu, T.-W. Chung, Equilibrium Isotherms of  
6 Volatile Alkanes, Alkenes, and Ketones on Activated Carbon, *J. Chem. Eng. Data.* 54 (2009)  
7 2208–2215. doi:10.1021/je800826d.
- 8 [20] L. Li, P.A. Quinlivan, D.R.U. Knappe, Effects of activated carbon surface chemistry and  
9 pore structure on the adsorption of organic contaminants from aqueous solution, *Carbon N.*



- 810 Y. 40 (2002) 2085–2100.
- 811 [21] N.J. Krou, I. Batonneau-Gener, T. Belin, S. Mignard, I. Javierre, I. Dubois-Brugger,  
812 Reactivity of volatile organic compounds with hydrated cement paste containing activated  
813 carbon, *Build. Environ.* 87 (2015) 102–107. doi:10.1016/j.buildenv.2015.01.025.
- 814 [22] M. Horgnies, E.M. Gartner, NO<sub>x</sub> de-pollution by hardened concrete and the influence of  
815 activated charcoal additions, *Cem. Concr. Res.* 42 (2012) 1348–1355.  
816 doi:10.1016/j.cemconres.2012.06.007.
- 817 [23] K. Jin, J. Miyawaki, N. Shiratori, S. Yoon, J. Jang, Toward an effective adsorbent for polar  
818 pollutants: Formaldehyde adsorption by activated carbon, *J. Hazard. Mater.* 260 (2013) 82–  
819 88. doi:10.1016/j.jhazmat.2013.04.049.
- 820 [24] J. Wu, D.D.L. Chung, Increasing the electromagnetic interference shielding effectiveness of  
821 carbon fiber polymer – matrix composite by using activated carbon fibers, *Carbon N. Y.* 40  
822 (2002) 445–447.
- 823 [25] G. Srinivas, Z.X. Guo, Graphene-based materials: Synthesis and gas sorption, storage and  
824 separation, *Prog. Mater. Sci.* 69 (2014) 1–60. doi:10.1016/j.pmatsci.2014.10.004.
- 825 [26] Q. Liu, Q. Xu, Q. Yu, R. Gao, T. Tong, Experimental investigation on mechanical and  
826 piezoresistive properties of cementitious materials containing graphene and graphene oxide  
827 nanoplatelets, *Constr. Build. Mater.* 127 (2016) 565–576.  
828 doi:10.1016/j.conbuildmat.2016.10.024.
- 829 [27] H. Du, S.D. Pang, Mechanical Response and Strain Sensing of Cement Composites Added  
830 with Graphene Nanoplatelet Under Tension, in: K. Sobolev, V. Shah (Eds.), *Nanotechnol.*  
831 *Constr.*, Springer, Cham, 2015: pp. 377–382. doi:10.1007/978-3-319-17088-6.
- 2 [28] A. Belli, A. Mobili, T. Bellezze, F. Tittarelli, P.B. Cachim, Evaluating the self-sensing ability  
3 of cement mortars manufactured with graphene nanoplatelets, virgin or recycled carbon  
4 fibers through piezoresistivity tests, *Sustainability.* 10 (2018) 4013. doi:10.3390/su10114013.
- 5 [29] S. Wen, D.D.L. Chung, Piezoresistivity-based strain sensing in carbon fiber-reinforced





- 836 cement, *ACI Mater. J.* 104 (2007) 171–179.
- 837 [30] X. Zhang, B. Gao, A. Elise, C. Cao, Y. Li, Adsorption of VOCs onto engineered carbon  
838 materials: A review, *J. Hazard. Mater.* 338 (2017) 102–123.  
839 doi:10.1016/j.jhazmat.2017.05.013.
- 840 [31] X. Zhen, W.C. Ng, Y.W. Tong, Y. Dai, K.G. Neoh, C.-H. Wang, Toxicity assessment of  
841 carbon black waste: A by-product from oil refineries, *J. Hazard. Mater.* 321 (2017) 600–610.  
842 doi:10.1016/j.jhazmat.2016.09.043.
- 843 [32] V.M. Harik, Geometry of carbon nanotubes and mechanisms of phagocytosis and toxic  
844 effects, *Toxicol. Lett.* 273 (2017) 69–85. doi:10.1016/j.toxlet.2017.03.016.
- 845 [33] R.A. Khushnood, S. Ahmad, P. Savi, J.M. Tulliani, M. Giorcelli, G.A. Ferro, Improvement  
846 in electromagnetic interference shielding effectiveness of cement composites using  
847 carbonaceous nano/micro inerts, *Constr. Build. Mater.* 85 (2015) 208–216.  
848 doi:10.1016/j.conbuildmat.2015.03.069.
- 849 [34] V. Benedetti, F. Patuzzi, M. Baratieri, Gasification char as a potential substitute of activated  
850 carbon in adsorption applications, *Energy Procedia.* 105 (2017) 712–717.  
851 doi:10.1016/j.egypro.2017.03.380.
- 852 [35] A. Sirico, P. Bernardi, B. Belletti, A. Malcevschi, E. Dalcanale, I. Domenichelli, P. Forni,  
853 E. Moretti, Mechanical characterization of cement-based materials containing biochar from  
854 gasification, *Constr. Build. Mater.* 246 (2020) 118490.  
855 doi:10.1016/j.conbuildmat.2020.118490.
- 856 [36] D. Maskell, C.F. da Silva, K. Mower, R. Cheta, A. Dengel, R. Ball, M. Ansell, P. Walker, A.  
857 Shea, Properties of bio-based insulation materials and their potential impact on indoor air  
8 quality, in: *First Int. Conf. Bio-Based Build. Mater.*, Clermont-Ferrand, France, 2015: pp. 1–  
9 8.
- 0 [37] C. Giosuè, A. Mobili, G. Toscano, M.L. Ruello, F. Tittarelli, Effect of Biomass Waste  
1 Materials as Unconventional Aggregates in Multifunctional Mortars for Indoor Application,



- 862           Procedia Eng. 161 (2016) 655–659. doi:10.1016/j.proeng.2016.08.724.
- 863   [38]   H. Bilal, M. Yaqub, S.K.U. Rehman, M. Abid, R. Alyousef, H. Alabduljabbar, F. Aslam,  
864           Performance of Foundry Sand Concrete under Ambient and Elevated Temperatures,  
865           Materials (Basel). 12 (2019) 2645. doi:10.3390/ma12162645.
- 866   [39]   R. Siddique, G. Singh, R. Belarbi, K. Ait-Mokhtar, Comparative investigation on the  
867           influence of spent foundry sand as partial replacement of fine aggregates on the properties of  
868           two grades of concrete, Constr. Build. Mater. 83 (2015) 216–222.  
869           doi:10.1016/j.conbuildmat.2015.03.011.
- 870   [40]   B. Bhardwaj, P. Kumar, Waste foundry sand in concrete: A review, Constr. Build. Mater.  
871           156 (2017) 661–674. doi:10.1016/j.conbuildmat.2017.09.010.
- 872   [41]   J. Válek, E. Van Halem, A. Viani, M. Pérez-Estébanez, R. Ševčík, P. Šašek, Determination  
873           of optimal burning temperature ranges for production of natural hydraulic limes, Constr.  
874           Build. Mater. 66 (2014) 771–780. doi:10.1016/j.conbuildmat.2014.06.015.
- 875   [42]   P. Faria, P. Duarte, D. Barbosa, I. Ferreira, New composite of natural hydraulic lime mortar  
876           with graphene oxide, Constr. Build. Mater. 156 (2017) 1150–1157.  
877           doi:10.1016/j.conbuildmat.2017.09.072.
- 878   [43]   M.M. Barbero-Barrera, N.F. Medina, C. Guardia-Martín, Influence of the addition of waste  
879           graphite powder on the physical and microstructural performance of hydraulic lime pastes,  
880           Constr. Build. Mater. 149 (2017) 599–611. doi:10.1016/j.conbuildmat.2017.05.156.
- 881   [44]   A. Mobili, C. Giosuè, T. Bellezze, G.M. Revel, F. Tittarelli, Gasification Char and Used  
882           Foundry Sand as Alternative Fillers to Graphene Nanoplatelets for Electrically Conductive  
883           Mortars with and without Virgin/Recycled Carbon Fibres, Appl. Sci. 11 (2021) 50.  
4           doi:10.3390/app11010050.
- 5   [45]   T.-C. Hou, V.K. Nguyen, Y.-M. Su, Y.-R. Chen, P.-J. Chen, Effects of coarse aggregates on  
6           the electrical resistivity of Portland cement concrete, Constr. Build. Mater. 133 (2017) 397–  
7           408. doi:10.1016/j.conbuildmat.2016.12.044.



- 888 [46] A. Mazzoli, O. Favoni, Particle size, size distribution and morphological evaluation of  
889 airborne dust particles of diverse woods by Scanning Electron Microscopy and image  
890 processing program, *Powder Technol.* 225 (2012) 65–71. doi:10.1016/j.powtec.2012.03.033.
- 891 [47] A. Mazzoli, G. Moriconi, Particle size, size distribution and morphological evaluation of  
892 glass fiber reinforced plastic (GRP) industrial by-product, *Micron.* 67 (2014) 169–178.  
893 doi:10.1016/j.micron.2014.07.007.
- 894 [48] H. Du, S.D. Pang, Enhancement of barrier properties of cement mortar with graphene  
895 nanoplatelet, *Cem. Concr. Res.* 76 (2015) 10–19. doi:10.1016/j.cemconres.2015.05.007.
- 896 [49] Y. Dai, M. Sun, C. Liu, Z. Li, Electromagnetic wave absorbing characteristics of carbon  
897 black cement-based composites, *Cem. Concr. Compos.* 32 (2010) 508–513.  
898 doi:10.1016/j.cemconcomp.2010.03.009.
- 899 [50] A. Mobili, C. Giosuè, V. Corinaldesi, F. Tittarelli, Bricks and Concrete Wastes as Coarse and  
900 Fine Aggregates in Sustainable Mortars, *Adv. Mater. Sci. Eng.* 2018 (2018).  
901 doi:10.1155/2018/8676708.
- 902 [51] A. Mobili, C. Giosuè, F. Tittarelli, Valorisation of GRP Dust Waste in Fired Clay Bricks,  
903 *Adv. Civ. Eng.* 2018 (2018). doi:10.1155/2018/5256741.
- 904 [52] F. Tittarelli, C. Giosuè, A. Mobili, M.L. Ruello, Influence of binders and aggregates on  
905 VOCs adsorption and moisture buffering activity of mortars for indoor applications, *Cem.*  
906 *Concr. Compos.* 57 (2015) 75–83. doi:10.1016/j.cemconcomp.2014.11.013.
- 907 [53] J. Cao, D.D.L. Chung, Coke powder as an admixture in cement for electromagnetic  
908 interference shielding, *Carbon N. Y.* 41 (2003) 2433–2436. doi:10.1016/S0008-  
909 6223(03)00289-6.
- 0 [54] S. Wen, D.D.L. Chung, Partial replacement of carbon fiber by carbon black in  
1 multifunctional cement-matrix composites, *Carbon N. Y.* 45 (2007) 505–513.  
2 doi:10.1016/j.carbon.2006.10.024.
- 3 [55] D.D.L. Chung, *Multifunctional Cement-Based Materials*, CRC Press, 2003.



- 914 [56] A. Belli, A. Mobili, T. Bellezze, F. Tittarelli, Commercial and recycled carbon/steel fibers  
915 for fiber-reinforced cement mortars with high electrical conductivity, *Cem. Concr. Compos.*  
916 109 (2020) 103569. doi:10.1016/j.cemconcomp.2020.103569.
- 917 [57] D.L. Lide, *Handbook of Chemistry and Physics*, 82nd ed., CRC Press, Boca Raton, Florida,  
918 USA, 2001.
- 919 [58] D.A. Hill, *Electromagnetic Theory of Reverberation Chambers*, NIST Technical Note 1506,  
920 National Institute of Standards and Technology, Boulder, Colorado, 1998.  
921 [http://ws680.nist.gov/publication/get\\_pdf.cfm?pub\\_id=24427](http://ws680.nist.gov/publication/get_pdf.cfm?pub_id=24427).
- 922 [59] D. Micheli, A. Vricella, R. Pastore, A. Delfini, R. Bueno Morles, M. Marchetti, F. Santoni,  
923 L. Bastianelli, F. Moglie, V. Mariani Primiani, V. Corinaldesi, A. Mazzoli, J. Donnini,  
924 *Electromagnetic properties of carbon nanotube reinforced concrete composites for frequency*  
925 *selective shielding structures*, *Constr. Build. Mater.* 131 (2017) 267–277.  
926 doi:10.1016/j.conbuildmat.2016.11.078.
- 927 [60] C.L. Holloway, D.A. Hill, J. Ladbury, G. Koepke, R. Garzia, *Shielding effectiveness*  
928 *measurements of materials using nested reverberation chambers*, *IEEE Trans. Electromagn.*  
929 *Compat.* 45 (2003) 350–356. doi:10.1109/TEM.2003.809117.
- 930 [61] M. Albano, D. Micheli, G. Gradoni, R.B. Morles, M. Marchetti, F. Moglie, V. Mariani  
931 Primiani, *Electromagnetic shielding of thermal protection system for hypersonic vehicles*,  
932 *Acta Astronaut.* 87 (2013) 30–39. doi:10.1016/j.actaastro.2013.02.003.
- 933 [62] L. Bastianelli, S. Capra, G. Gradoni, D. Micheli, A. Vricella, V. Corinaldesi, A. Mazzoli, F.  
934 Moglie, V.M. Primiani, *Shielding effectiveness statistical evaluation of random concrete*  
935 *composites*, in: *3rd IEEE Int. Work. Metrol. Aerospace, MetroaeroSp., IEEE*, 2016: pp. 172–  
6 176. doi:10.1109/MetroAeroSpace.2016.7573207.
- 7 [63] D.A. Hill, *Electronic Mode Stirring for Reverberation Chambers*, *IEEE Trans. Electromagn.*  
8 *Compat.* 36 (1994) 294–299. doi:10.1109/15.328858.
- 9 [64] S. Monosi, F. Tittarelli, C. Giosuè, M.L. Ruello, *Effect of two different sources and washing*



- 940 treatment on the properties of UFS by-products for mortar and concrete production, *Constr.*  
941 *Build. Mater.* 44 (2013) 260–266. doi:10.1016/j.conbuildmat.2013.02.029.
- 942 [65] K. Gong, S.M. Asce, Z. Pan, A.H. Korayem, D. Ph, L. Qiu, D. Li, F. Collins, C.M. Wang,  
943 W.H. Duan, a M. Asce, Reinforcing Effects of Graphene Oxide on Portland Cement Paste, *J.*  
944 *Mater. Civ. Eng.* vol 27 (2014) 1–6. doi:10.1061/(ASCE)MT.1943-5533.0001125.
- 945 [66] S. Gupta, H.W. Kua, Carbonaceous micro-filler for cement: Effect of particle size and dosage  
946 of biochar on fresh and hardened properties of cement mortar, *Sci. Total Environ.* 662 (2019)  
947 952–962. doi:10.1016/j.scitotenv.2019.01.269.
- 948 [67] C. Giosuè, A. Mobili, B. Citterio, F. Biavasco, M.L. Ruello, F. Tittarelli, Innovative  
949 hydraulic lime-based finishes with unconventional aggregates and TiO<sub>2</sub> for the improvement  
950 of indoor air quality, *Manuf. Rev.* 7 (2020) 1–9. doi:10.1051/mfreview/2020010.
- 951 [68] M. Collepardi, *The new concrete*, Tintoretto, Castrette di Villorba, Italy, 2006.
- 952 [69] T. Oey, A. Kumar, J.W. Bullard, N. Neithalath, G. Sant, The filler effect: The influence of  
953 filler content and surface area on cementitious reaction rates, *J. Am. Ceram. Soc.* 96 (2013)  
954 1978–1990. doi:10.1111/jace.12264.
- 955 [70] J. Vera-Agullo, V. Chozas-Ligero, D. Portillo-Rico, M. García-Casas, A. Gutiérrez-Martínez,  
956 J. Mieres-Royo, J. Grávalos-Moreno, Mortar and Concrete Reinforced with Nanomaterials,  
957 in: Z. Bittnar, P. Bartos, J. Němeček, V. Šmilauer, J. Zeman (Eds.), *Nanotechnol. Constr.* 3,  
958 Springer, Berlin, Heidelberg, 2009: pp. 383–388. doi:10.1007/978-3-642-00980-8\_52.
- 959 [71] H. Moosberg-Bustnes, B. Lagerblad, E. Forsberg, The function of fillers in concrete, *Mater.*  
960 *Struct.* 37 (2004) 74–81. doi:10.1617/13694.
- 961 [72] E. Berodier, K. Scrivener, Understanding the filler effect on the nucleation and growth of C-  
2 S-H, *J. Am. Ceram. Soc.* 97 (2014) 3764–3773. doi:10.1111/jace.13177.
- 3 [73] R.T. Yang, *Gas Separation by Adsorption Processes*, Butterworth Publishers, Stoneham,  
4 1987.
- 5 [74] M. Gonçalves, M. Molina-Sabio, F. Rodriguez-Reinoso, Modification of activated carbon



- 966 hydrophobicity by pyrolysis of propene, *J. Anal. Appl. Pyrolysis*. 89 (2010) 17–21.  
967 doi:10.1016/j.jaap.2010.04.009.
- 968 [75] S. Ranjan, D. Nandita, E. Lichtfouse, *Nanoscience in Food and Agriculture 1*, Springer  
969 Nature, 2016. doi:10.1007/978-3-319-39303-2.
- 970 [76] M. Zhang, Y. Ma, Y. Zhu, J. Che, Y. Xiao, Two-dimensional transparent hydrophobic  
971 coating based on liquid-phase exfoliated graphene fluoride, *Carbon N. Y.* 63 (2013) 149–  
972 156. doi:10.1016/j.carbon.2013.06.066.
- 973 [77] S.G. Prolongo, R. Moriche, A. Jiménez-Suárez, M. Sánchez, A. Ureña, Advantages and  
974 disadvantages of the addition of graphene nanoplatelets to epoxy resins, *Eur. Polym. J.* 61  
975 (2014) 206–214. doi:10.1016/j.eurpolymj.2014.09.022.
- 976 [78] Y. Benachour, C.A. Davy, F. Skoczylas, H. Houari, Effect of a high calcite filler addition  
977 upon microstructural, mechanical, shrinkage and transport properties of a mortar, *Cem.*  
978 *Concr. Res.* 38 (2008) 727–736. doi:10.1016/j.cemconres.2008.02.007.
- 979 [79] S. Monosi, D. Sani, F. Tittarelli, Used Foundry Sand in Cement Mortars and Concrete  
980 Production, *Open Waste Manag. J.* 3 (2010) 18–25. doi:10.2174/1876400201003010018.
- 981 [80] F. Çeçen, A. Özgür, *Activated carbon for water and wastewater treatment: Integration of*  
982 *adsorption and biological treatment*, John Wiley & Sons, 2011.
- 983 [81] K.J. Lee, J. Miyawaki, N. Shiratori, S.H. Yoon, J. Jang, Toward an effective adsorbent for  
984 polar pollutants: Formaldehyde adsorption by activated carbon, *J. Hazard. Mater.* 260 (2013)  
985 82–88. doi:10.1016/j.jhazmat.2013.04.049.
- 986 [82] A.H. Mamaghani, F. Haghghat, C.-S. Lee, Photocatalytic oxidation technology for indoor  
987 environment air purification: The state-of-the-art, *Appl. Catal. B Environ.* 203 (2017) 247–  
8 269. doi:10.1016/j.apcatb.2016.10.037.
- 9 [83] C. Giosuè, M. Pierpaoli, A. Mobili, M.L. Ruello, F. Tittarelli, **Multifunctional Lightweight**  
0 **Mortars for Indoor Applications to Improve Comfort and Health of Occupants : Thermal**  
1 **Properties and Photocatalytic Efficiency**, *Front. Mater.* 7 (2020) 1–10.



992 [doi:10.3389/fmats.2020.00255](https://doi.org/10.3389/fmats.2020.00255).

- 993 [84] V. Georgakilas, M. Otyepka, A.B. Bourlinos, V. Chandra, N. Kim, K.C. Kemp, P. Hobza, R.  
994 Zboril, K.S. Kim, Functionalization of graphene: Covalent and non-covalent approaches,  
995 derivatives and applications, *Chem. Rev.* 112 (2012) 6156–6214. doi:10.1021/cr3000412.
- 996 [85] H. Zhang, X. Lv, Y. Li, Y. Wang, J. Li, P25- graphene composite as a high performance  
997 photocatalyst, *ACS Nano.* 4 (2009) 380–386. doi:10.1021/nn901221k.
- 998 [86] X.-Y. Zhang, Graphene/TiO<sub>2</sub> nanocomposites: synthesis, characterization and application in  
999 hydrogen evolution from water photocatalytic splitting, *J. Mater. Chem.* 20 (2010) 2801–  
1000 2806. doi:10.1039/b917240h.
- 1001 [87] D. Enea, G.L. Guerrini, Photocatalytic Properties of Cement-Based Plasters and Paints  
1002 Containing Mineral Pigments, *Transp. Res. Rec. J. Transp. Res. Board.* (2010) pp 52--60.  
1003 doi:10.3141/2141-10.
- 1004 [88] W.. Daoud, *Self-Cleaning Materials and Surfaces: A Nanotechnology Approach*, John Wiley  
1005 & Sons, 2013. doi:10.1002/9781118652336.
- 1006 [89] J. Chen, C. Poon, Photocatalytic activity of titanium dioxide modified concrete materials –  
1007 Influence of utilizing recycled glass cullets as aggregates, *J. Environ. Manage.* 90 (2009)  
1008 3436–3442. doi:10.1016/j.jenvman.2009.05.029.
- 1009 [90] A. Al-Dahawi, O. Öztürk, F. Emami, G. Yildirim, M. Şahmaran, Effect of mixing methods  
1010 on the electrical properties of cementitious composites incorporating different carbon-based  
1011 materials, *Constr. Build. Mater.* 104 (2016) 160–168.  
1012 doi:10.1016/j.conbuildmat.2015.12.072.
- 1013 [91] A. Belli, A. Mobili, T. Bellezze, F. Tittarelli, P.B. Cachim, Piezoresistive behavior of  
4 mortars loaded with graphene and carbon fibers for the development of self-sensing  
5 composites, in: *Adv. Trends Eng. Sci. Technol. III- Proc. 3rd Int. Conf. Eng. Sci. Technol.*,  
6 Taylor & Francis Group, 2019: pp. 37–42.
- 7 [92] D.D.L. Chung, Dispersion of Short Fibers in Cement, *J. Mater. Civ. Eng.* 17 (2005) 379–383.



- 1018 doi:10.1061/(ASCE)0899-1561(2005)17:4(379).
- 1019 [93] A. Samková, P. Kulhavý, M. Pechočiaková, Possibilities to improve electromagnetic  
1020 shielding of plaster composites adding carbon fibers, IOP Conf. Ser. Mater. Sci. Eng. 254  
1021 (2017) 042025. doi:10.1088/1757-899X/254/4/042025.
- 1022 [94] X. Lv, Y. Duan, G. Chen, Electromagnetic wave absorption properties of cement-based  
1023 composites filled with graphene nano-platelets and hollow glass microspheres, Constr. Build.  
1024 Mater. 162 (2018) 280–285. doi:10.1016/j.conbuildmat.2017.12.047.
- 1025 [95] A.P. Singh, M. Mishra, A. Chandra, S.K. Dhawan, Graphene oxide/ferrofluid/cement  
1026 composites for electromagnetic interference shielding application, Nanotechnology. 22  
1027 (2011) 465701. doi:10.1088/0957-4484/22/46/465701.
- 1028 [96] A. Mahmood, R. Arsalan, M. Zeeshan, Pyrolytic carbonaceous reinforcements for enhanced  
1029 electromagnetic and fracture response of cementitious composites, J. Clean. Prod. 248 (2020)  
1030 119288. doi:10.1016/j.jclepro.2019.119288.
- 1031

